ENGINEERING OF
BIOMATERIALS
INŻYNIERIA BIOMATERIAŁÓW
JOURNAL OF POLISH SOCIETY FOR BIOMATERIALS AND FACULTY OF MATERIALS SCIENCE AND CERAMICS AGH-UST
CZASOPISMO POLSKIEGO STOWARZYSZENIA BIOMATERIAŁÓW I WYDZIAŁU INŻYNIERII MATERIAŁOWEJ I CERAMIKI AGH

Number 149
Numer 149
Volume XXII
Rok XXII

JANUARY 2019
STYCZEŃ 2019

ISSN 1429-7248

PUBLISHER:
WYDAWCA:

Polish Society for Biomaterials in Krakow
Polskie Stowarzyszenie Biomateriałów w Krakowie

ADDRESS OF EDITORIAL OFFICE:
ADRES REDAKCJI:

AGH-UST
30/A3, Mickiewicz Av.
30-059 Krakow, Poland
Akademia Górniczo-Hutnicza
al. Mickiewicza 30/A-3
30-059 Kraków

Issue: 250 copies
Nakład: 250 egz.

Scientific Publishing House AKAPIT
Wydawnictwo Naukowe AKAPIT
e-mail: wn@akapit.krakow.pl

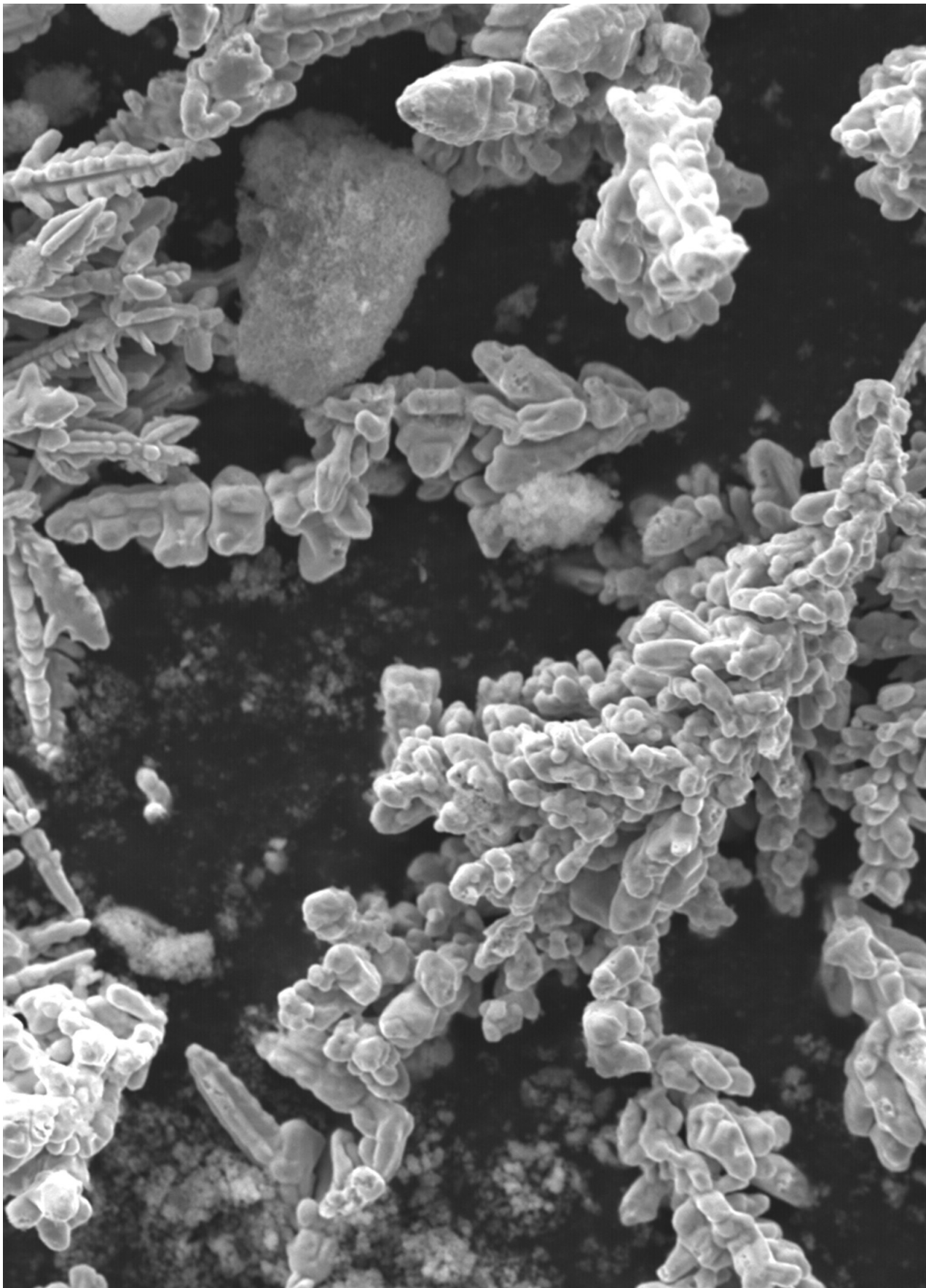

ENGINEERING OF BIOMATERIALS

EDITORIAL BOARD
KOMITET REDAKCYJNY

INTERNATIONAL EDITORIAL BOARD
MIĘDZYNARODOWY KOMITET REDAKCYJNY

ENGINEERING OF BIOMATERIALS

Wskazówki dla autorów

1. Prace do opublikowania w kwartalniku „Engineering of Biomaterials / Inżynieria Biomateriałów" przyjmowane będą wyłącznie w języku angielskim. Możliwe jest również dołączenie dodatkowo polskiej wersji językowej.
2. Wszystkie nadsyłane artykuły są recenzowane.
3. Materiały do druku prosimy przysyłać na adres e-mail: kabe@agh.edu.pl.
4. Struktura artykułu:
• TYTUŁ • Autorzy i instytucje • Streszczenie (200-250 słów) • Słowa kluczowe (4-6) • Wprowadzenie • Materiały i metody • Wyniki i dyskusja • Wnioski • Podziękowania • Piśmiennictwo
5. Autorzy przesyłają pełną wersję artykułu, łącznie z ilustracjami, tabelami, podpisami i literaturą w jednym pliku. Artykuł w tej formie przesyłany jest do recenzentów. Dodatkowo autorzy proszeni są o przesłanie materiałów ilustracyjnych (rysunki, schematy, fotografie, wykresy) w oddzielnych plikach (format np. .jpg, .gif., .tiff, .bmp). Rozdzielczość rysunków min. 300 dpi. Wszystkie rysunki i wykresy powinny być czarno-białe lub w odcieniach szarości i ponumerowane cyframi arabskimi. W tekście należy umieścić odnośniki do rysunków i tabel. W przypadku artykułów dwujęzycznych w tabelach i na wykresach należy umieścić opisy polskie i angielskie.
6. Na końcu artykułu należy podać wykaz piśmiennictwa w kolejności cytowania w tekście i kolejno ponumerowany.
7. Redakcja zastrzega sobie prawo wprowadzenia do opracowań autorskich zmian terminologicznych, poprawek redakcyjnych, stylistycznych, w celu dostosowania artykułu do norm przyjętych w naszym czasopiśmie. Zmiany i uzupełnienia merytoryczne będą dokonywane w uzgodnieniu z autorem.
8. Opinia lub uwagi recenzentów będą przekazywane Autorowi do ustosunkowania się. Nie dostarczenie poprawionego artykułu w terminie oznacza rezygnację Autora z publikacji pracy w naszym czasopiśmie.
9. Za publikację artykułów redakcja nie płaci honorarium autorskiego.
10. Adres redakcji:

Czasopismo
„Engineering of Biomaterials / Inżynieria Biomateriałów"
Akademia Górniczo-Hutnicza im. St. Staszica
Wydział Inżynierii Materiałowej i Ceramiki
al. Mickiewicza 30/A-3, 30-059 Kraków
tel. (48) 12 617 25 03, 12 617 25 61
tel./fax: (48) 12 617 45 41
e-mail: chlopek@agh.edu.pl, kabe@agh.edu.pl

Szczegółowe informacje dotyczące przygotowania manuskryptu oraz procedury recenzowania dostępne są na stronie internetowej czasopisma:
www.biomat.krakow.pl

Warunki prenumeraty

Zamówienie na prenumeratę prosimy przesyłać na adres:
mgr inż. Augustyn Powroźnik
apowroz@agh.edu.pl, tel/fax: (48) 12 617 45 41
Cena pojedynczego numeru wynosi 20 PLN
Konto: Polskie Stowarzyszenie Biomateriałów
30-059 Kraków, al. Mickiewicza 30/A-3
ING Bank Śląski S.A. O/Kraków
nr rachunku 63 1050 1445 1000 0012 0085 6001

Prenumerata obejmuje 4 numery regularne i nie obejmuje numeru specjalnego (materiały konferencyjne).

Instructions for authors

1. Papers for publication in quarterly journal „Engineering of Biomaterials / Inżynieria Biomateriałów" should be written in English.
2. All articles are reviewed.
3. Manuscripts should be submitted to editorial office by e-mail to kabe@agh.edu.pl.
4. A manuscript should be organized in the following order:
• TITLE • Authors and affiliations • Abstract (200-250 words) • Keywords (4-6) • Introduction • Materials and Methods • Results and Discussions • Conclusions • Acknowledgements • References
5. All illustrations, figures, tables, graphs etc. preferably in black and white or grey scale should be additionally sent as separate electronic files (format .jpg, .gif., .tiff, .bmp). High-resolution figures are required for publication, at least 300 dpi. All figures must be numbered in the order in which they appear in the paper and captioned below. They should be referenced in the text. The captions of all figures should be submitted on a separate sheet.
6. References should be listed at the end of the article. Number the references consecutively in the order in which they are first mentioned in the text.
7. The Editors reserve the right to improve manuscripts on grammar and style and to modify the manuscripts to fit in with the style of the journal. If extensive alterations are required, the manuscript will be returned to the authors for revision.
8. Opinion or notes of reviewers will be transferred to the author. If the corrected article will not be supplied on time, it means that the author has resigned from publication of work in our journal.
9. Editorial does not pay author honorarium for publication of article.
10. Address of editorial office:

Journal
„Engineering of Biomaterials / Inżynieria Biomateriałów"
AGH University of Science and Technology
Faculty of Materials Science and Ceramics
30/A-3, Mickiewicz Av., 30-059 Krakow, Poland
tel. (48) 12) 617 25 03, 12 617 25 61
tel./fax: (48) 12 617 45 41
e-mail: chlopek@agh.edu.pl, kabe@agh.edu.pl

Detailed information concerning manuscript preparation and review process are available at the journal's website:
www.biomat.krakow.pl

Subscription terms

Contact:
MSc Augustyn Powroźnik,
e-mail: apowroz@agh.edu.pl
Subscription rates:
Cost of one number: 20 PLN
Payment should be made to:
Polish Society for Biomaterials
30/A3, Mickiewicz Av.
30-059 Krakow, Poland
ING Bank Slaski S.A.
account no. 63 1050 1445 1000 0012 0085 6001

Subscription includes 4 issues and does not include special issue (conference materials).

28th Biomaterials in Medicine and Veterinary Medicine

Annual Conference

10 – 13 October 2019 Rytro, Poland

SAVE THE DATE

10-13

OCTOBER

2019

www.biomat.agh.edu.pl

REGISTER

AND

SUBMIT

AN ABSTRACT

STUDIA PODYPLOMOWE

Biomateriały – Materiały dla Medycyny

2019/2020

Organizator: Akademia Górniczo-Hutnicza im. Stanisława Staszica w Krakowie Wydział Inżynierii Materiałowej i Ceramiki Katedra Biomateriałów i Kompozytów **Kierownik:** prof. dr hab. inż. Elżbieta Pamuła **Sekretarz:** dr inż. Małgorzata Krok-Borkowicz	**Adres:** 30-059 Kraków, Al. Mickiewicza 30 Pawilon A3, p. 208, 210 lub 501 tel. 12 617 44 48, 12 617 23 38, fax. 12 617 33 71 email: epamula@agh.edu.pl; krok@agh.edu.pl https://www.agh.edu.pl/ksztalcenie/oferta-ksztalcenia/studia-podyplomowe-kursy-doksztalcajace-i-szkolenia/biomaterialy-materialy-dla-medycyny/

Charakterystyka:
Tematyka prezentowana w trakcie zajęć obejmuje przegląd wszystkich grup materiałów dla zastosowań medycznych: metalicznych, ceramicznych, polimerowych, węglowych i kompozytowych. Słuchacze zapoznają się z metodami projektowania i wytwarzania biomateriałów a następnie możliwościami analizy ich właściwości mechanicznych, właściwości fizykochemicznych (laboratoria z metod badań: elektronowa mikroskopia skaningowa, mikroskopia sił atomowych, spektroskopia w podczerwieni, badania energii powierzchniowej i zwilżalności) i właściwości biologicznych (badania: *in vitro* i *in vivo*). Omawiane są regulacje prawne i aspekty etyczne związane z badaniami na zwierzętach i badaniami klinicznymi (norma EU ISO 10993). Słuchacze zapoznają się z najnowszymi osiągnięciami w zakresie nowoczesnych nośników leków, medycyny regeneracyjnej i inżynierii tkankowej.

Sylwetka absolwenta:
Studia adresowane są do absolwentów uczelni technicznych (inżynieria materiałowa, technologia chemiczna), przyrodniczych (chemia, biologia, biotechnologia) a także medycznych, stomatologicznych, farmaceutycznych i weterynaryjnych, pragnących zdobyć, poszerzyć i ugruntować wiedzę z zakresu inżynierii biomateriałów i nowoczesnych materiałów dla medycyny. Słuchacze zdobywają i/lub pogłębiają wiedzę z zakresu inżynierii biomateriałów. Po zakończeniu studiów wykazują się znajomością budowy, właściwości i sposobu otrzymywania materiałów przeznaczonych dla medycyny. Potrafią analizować wyniki badań i przekładać je na zachowanie się biomateriału w warunkach żywego organizmu. Ponadto słuchacze wprowadzani są w zagadnienia dotyczące wymagań normowych, etycznych i prawnych niezbędnych do wprowadzenia nowego materiału na rynek. Ukończenie studiów pozwala na nabycie umiejętności przygotowywania wniosków do Komisji Etycznych i doboru metod badawczych w zakresie analizy biozgodności materiałów.

Zasady naboru:
Termin zgłoszeń: od 20.09.2019 do 20.10.2019 (liczba miejsc ograniczona - decyduje kolejność zgłoszeń)
Wymagane dokumenty: dyplom ukończenia szkoły wyższej
Osoby przyjmujące zgłoszenia:
prof. dr hab. inż. Elżbieta Pamuła (pawilon A3, p. 208, tel. 12 617 44 48, e-mail: epamula@agh.edu.pl)
dr inż. Małgorzata Krok-Borkowicz (pawilon A3, p. 210, tel. 12 617 23 38, e-mail: krok@agh.edu.pl)

Czas trwania: 2 semestry (od XI 2019 r. do VI 2020 r.) 8 zjazdów (soboty-niedziele) 1 raz w miesiącu	**Opłaty:** 2 600 zł (za dwa semestry)

SPIS TREŚCI
CONTENTS

Wersja papierowa czasopisma „Engineering of Biomaterials / Inżynieria Biomateriałów" jest jego wersją pierwotną
Printed version of „Engineering of Biomaterials / Inżynieria Biomateriałów" is a primary version of the journal

PHENOLIC PLANT EXTRACT ENRICHMENT OF ENZYMATICALLY MINERALIZED HYDROGELS

Timothy E.L. Douglas[1,2,3*], Marco A. Lopez-Heredia[4], Aleksandra Pułczyńska[5], Agata Łapa[5], Krzysztof Pietryga[5], David Schaubroeck[6], Sónia A.O. Santos[7], Adriana Pais[7], Gilles Brackman[8], Karel De Schamphelaere[9], Sangram Keshari Samal[10,11], Julia K. Keppler[12], Jonas L. Bauer[12], Feng Chai[4], Nicolas Blanchemain[4], Tom Coenye[8], Elżbieta Pamuła[5], Andre G. Skirtach[1,11]

[1] Dept. Molecular Biotechology, Ghent University, Belgium
[2] Engineering Department, Lancaster University, United Kingdom
[3] Material Science Institute (MSI), Lancaster University, United Kingdom
[4] U1008: Controlled Drug Delivery Systems and Biomaterials, Univ. Lille II, France
[5] Dept. Biomaterials and Composites, AGH University of Science and Technology, Kraków, Poland
[6] Centre for Microsystems Technology (CMST), imec and Ghent University, Belgium
[7] CICECO-Aveiro Institute of Materials, Dept. Chemistry, University of Aveiro, Portugal
[8] Laboratory of Pharmaceutical Microbiology, Ghent University, Belgium
[9] Laboratory for Environmental and Acquatic Ecology, Ghent University, Belgium
[10] Laboratory of General Biochemistry and Physical Pharmacy, Ghent University, Belgium
[11] Centre for Nano- and Biophotonics, Ghent University, Belgium,
[12] Dept. Food Technology, Christian-Albrechts-Universität zu Kiel, Germany
*e-mail: t.douglas@lancaster.ac.uk

Abstract

Hydrogel mineralization with calcium phosphate (CaP) and antibacterial activity are desirable for applications in bone regeneration. Mineralization with CaP can be induced using the enzyme alkaline phosphatase (ALP), responsible for CaP formation in bone tissue. Incorporation of polyphenols, plant-derived bactericidal molecules, was hypothesized to provide antibacterial activity and enhance ALP-induced mineralization. Three phenolic rich plant extracts from: (i) green tea, rich in epigallocatechin gallate (EGCG) (herafter referred to as EGCG-rich extract); (ii) pine bark and (iii) rosemary were added to gellan gum (GG) hydrogels and subsequently mineralized using ALP. The phenolic composition of the three extracts used were analyzed by ultra-high-performance liquid chromatography coupled to tandem mass spectrometry (UHPLC-MS^n). EGCG-rich extract showed the highest content of phenolic compounds and promoted the highest CaP formation as corroborated by dry mass percentage meassurements and ICP-OES determination of mass of elemental Ca and P. All three extracts alone exhibited antibacterial activity in the following order EGCG-rich > PI > RO, respectively. However, extract-loaded and mineralized GG hydrogels did not exhibit appreciable antibacterial activity by diffusion test. In conclusion, only the EGCG-rich extract promotes ALP-mediated mineralization.

Keywords: *hydrogel, mineralization, polyphenols, antibacterial, epigallocatechin gallate, gellan gum*

[Engineering of Biomaterials 149 (2019) 2-9]

Introduction

Hydrogels are 3D polymer structures, or networks, in which a high amount of liquid is introduced [1]. These materials present the advantage of being loaded with active molecules, drugs and/or cells. In addition, the properties of hydrogels can be tailored by modifying the polymer network composing the hydrogel or their cross-linking mechanism [2,3]. Gellan Gum (GG) is made of polysaccharide anionic polymer which can be used as the networks for obtaining hydrogels [4,5]. Mineralization of this type of hydrogels with calcium phosphate (CaP) is desirable for applications in bone regeneration. One mineralization strategy is incorporation of the enzyme alkaline phosphatase (ALP) to cleave phosphate from glycerophosphate (GP) substrate upon incubation in a solution containing Ca^{2+} and GP, resulting in CaP formation in the hydrogel [6].

In addition to this mineralization capacity, antibacterial properties are desirable for bone regeneration materials as the increasing prevalence of antibiotic-resistant bacteria, *e.g.* methicillin-resistant *Staphylococcus aureus* Mu50 (MRSA), is a major concern in clinic [7,8]. Flavonoids, *i.e.* a sub-class of polyphenols occurring in fruit, vegetables, nuts, seeds, stems, flowers and tea, exhibit antibacterial activity in addition to other properties such as antioxidant, anti-inflammatory, anti-mutagenic and anti-carcinogenic properties [9,10]. The mechanism of action of several flavonoids has been investigated [9], being known that their structure and concentration can affect the ALP and cell activities [11]. Previously, incorporation of a macroalgae phenolic extract into GG hydrogels promoted subsequent ALP-induced mineralization and endowed antibacterial activity before and after mineralization [6]. Quercetin and apigenin have been object of particular interest amongst flavonoids due to their antibacterial properties [10].

In this work, two well-known plant extracts, namely green tea extract, rich in epigallocatechin gallate (EGCG), hereafter referred to EGCG-rich extract, and rosemary extract (RO), and a less studied extract, i.e. pine bark (PI, Pycnogenol) were added to GG hydrogels. GG hydrogels were subsequently mineralized using ALP. We hypothesized that these extracts would promote CaP formation and endow antibacterial activity. In fact, green tea extract has shown antibacterial activity against both Gram-positive and Gram-negative bacteria [12]. Pine bark and rosemary extracts have been also reported to show antibacterial activity, ascribed by the authors to the presence of polyphenols [13], and phenolic acids [14], respectively. Notwithstanding, green tea, rosemary and pine bark extracts were characterized by ultra-high-performance liquid chromatography with diode array detector and coupled to an ion trap mass spectrometer (UHPLC-DAD-MS^n). Promotion of mineralization was assessed by measurement of dry mass percentage, *i.e.* mass percentage of mineralized hydrogels attributable to mineral and polymer and not water, by Inductively Coupled Plasma Optical Emission Spectroscopy (ICP-OES), Fourier Transform Infrared Spectroscopy (FTIR) and Scanning Electron Microscopy (SEM) analysis. Antibacterial activity was tested against three commonly occurring bacteria known to colonize biomaterials, *i.e.* MRSA, *Staphylococcus aureus* and *Escherichia coli.*

Materials and methods

Materials

All materials, including GG (G1910, "Low-Acyl", 200-300 kD), calcium glycerophosphate (CaGP, 50043) and alkaline phosphatase (P7640), formic acid (purity >98%) gallic acid (purity >97.5%), catechin (purity >96%), caffeic acid (purity >95%), chlorogenic acid (purity >95%), luteolin (purity >98%), naringenin (98% purity), isorhamnetin (99% purity) were acquired from Sigma-Aldrich, unless stated otherwise. HPLC-grade methanol, water and acetonitrile were supplied by Fisher Scientific Chemicals (Loures, Portugal) and further filtered using a Solvent Filtration Apparatus 58061 from Supelco (Bellefonte, PA, USA). EGCG-rich extract (Green tea polyphenol extract, extracted by liquid/solid extraction, using water as solvent for the extraction, followed by purification with ethanol. EGCG > 65% (according to specification and information from manufacturer) was obtained from Oskar Tropitzsch e. K. Germany, PI extract (Pycnogenol®, from *Pinus pinaster*) was acquired from Biolandes Arômes, France and RO extract (Aquarox®, from *Rosmarinus officinalis*) from Vitiva, Slovenia.

Extract analysis

Extracts were analyzed by UHPL-DAD-MS^n. Extracts were dissolved in methanol HPLC grade (2–10 mg/mL) and filtered through a 0.2 µm PTFE syringe filter before injection (5 µL). The UHPLC system comprised a variable loop Accela autosampler (15°C), Accela 600 LC pump and Accela 80 Hz PDA detector (Thermo Fisher Scientific, San Jose, CA, USA). Compound separation was performed using a Hypersil Gold C_{18} (100 mm × 2.1 mm × 1.9 µm) column (Thermo Scientific, U.S.A.), at a flow rate of 0.42 mL/min and at 45°C. Mobile phase consisted of water/acetonitrile (99:1, v/v) (A) and acetonitrile (B), both with 0.1% formic acid. The following linear gradient was applied: 0-3 min: 1% B; 3-6 min: 1-5% B; 6-12 min: 5-10% B; 12-15 min: 10-15% B; 15-17 min: 15% B; 17-22 min: 15-20% B; 22-27 min: 20-25% B; 27-29 min: 25-50% B; 29-31 min: 50-100% B; 31-32 min: 100% B; 32-36 min: 100-1% B; followed by 4 min re-equilibration. Chromatograms at 280, 320 and 340 nm, and UV spectra from 200 to 600 nm were recorded.

UHPLC was coupled to a LCQ Fleet ion trap mass spectrometer (ThermoFinnigan, San Jose, CA, USA), as described before [15]. Capillary temperature was 275ºC and capillary and tune lens voltages were -41 V and -75 V, respectively.

Hydrogel preparation

GG hydrogel discs loaded with ALP and extract were prepared as described before [6] (FIG. 1a) and had final concentrations of 0.7% (w/v) GG, 0.03% (w/v) $CaCl_2$, 2.5 mg/mL ALP and 2.5 mg/mL of extract and were of 6 mm in diameter and 2.5 mm in height. GG, 0.1 M CaGP and ddH_2O were sterilized by autoclaving, $CaCl_2$, ALP and extract solutions by filtration (pore diameter 0.22 µm). ALP- and extract-loaded hydrogels were incubated in 0.1 M CaGP for 5 days (with refreshment after 1 and 3 days). Dry mass percentage was calculated as [(sample mass after drying)/(sample mass before drying)]x100%. SEM, ICP-OES and FTIR were performed as described before [6,16].

Antibacterial properties

For the minimal inhibitory concentration (MIC) test, MRSA was cultured in Mueller-Hinton broth (MH; Oxoid, Basingstoke, UK) at 37°C in aerobic conditions. The EUCAST broth microdilution protocol was used with flat-bottom 96-well plates (TPP, Trasadingen, Switzerland). The inoculum was standardized to approximately 5×10^5 Colony Forming Units (CFU)/mL. Extract concentrations ranging from 1024 µg/mL to 0.5 µg/mL were examined. After incubation at 37°C for 24 h, optical density was measured at 590 nm. MIC was defined as the lowest extract concentration at which the inoculated and the blank wells displayed similar optical densities.

After determining bactericidal activity by MIC measurement, antibacterial properties of the ALP- and extract loaded hydrogels post-mineralization were tested using the Kirby-Bauer diffusion test [17]. A hydrogel was placed in the middle of a 9 cm diameter Petri dish. 18 mL Mueller-Hinton agar (MHA) containing $1x10^7$ CFU/mL bacteria solidified in the dish over the hydrogel. After 24 h incubation under aerobic conditions at 37°C, the diameter of the inhibition growth zone was measured. *E. coli* (L70A4), *MRSA* (07001) and *S. aureus* (CIP224) were used.

Results and Discussion

Characteristics of extracts by UHPLC-DAD-MS^n

The phenolic fraction of EGCG-rich, PI and RO extracts were detailed characterized by UHPLC-DAD-MS^n analysis (TABLE 1). Phenolic compounds were identified based on their retention time, UV spectra and MS^n fragmentation pathway, comparing them with reference compounds or, when these were not available, with the literature. Quantification was performed using calibration curves of standards representative of each phenolic compound family (TABLE 2).

One phenolic acid and six flavanols were identified in EGCG-rich extract, namely gallic acid, two (epi)gallocatechin (EGC) isomers, catechin, two (epi)gallocatechin gallate (EGCG) isomers and (epi)catechin gallate (ECG) (TABLE 1). (Epi)gallocatechin gallate (EGCG) isomers were the major components found, accounting for 387.20 ± 15.53 mg/g and 181.96 ± 6.73 mg/g of the extract, respectively (TABLE 3). These results are consistent with the findings of Del Rio et al [23]. PI extract was shown to consist of quinic acid, protocatechuic acid, two B-type proanthocyanidin dimer isomers, catechin, caffeic acid, taxifolin-*O*-hexoside and taxifolin (TABLE 1). These compounds are well known constituents of pine bark extracts [24,25]. Quinic acid (26.95 ± 0.92 mg/g of the extract) and one B-type proanthocyanidin dimer (6.05 ± 0.44 mg/g of the extract) were shown to be the major components (TABLE 3).

In the same way, eighteen components were identified in RO extract (TABLE 1), namely quinic, syringic and caffeic and chlorogenic acids and three luteolin-*O*-rutinoside isomers, rosmarinic acid-glucoside, isorhamnetin-3-*O*-hexoside, apigenin-7-*O*-glucoside, rosmarinic acid, hesperetin-7-*O*-rutinoside, luteolin-7-*O*-glucuronide, three luteolin-3-*O*-(2''-*O*-acetyl)-b-D-glucuronide isomers, isorhamnetin-*O*-rutinoside and apigenin. Hesperetin-7-*O*-rutinoside and apigenin-7-*O*-glucoside were shown to be the major components of RO extract, accounting for 43.14 ± 1.09 mg/g and 20.16 ± 1.00 mg/g of the extract, respectively (TABLE 3). This in contrast to the findings of other authors who reported rosmarinic acid, carnosol and carnosic acid as the major compounds of rosemary extract [14,26]. Considering the total content of phenolic compounds, EGCG-rich extract showed the highest content (635.31 ± 19.31 mg/g of extract), followed by RO extract (112.59 ± 2.60 mg/g of extract) and by PI extract (49.99 ± 0.82 mg/g of extract).

TABLE 1. Phenolic compounds identified in EGCG-rich, PI and RO extracts and their corresponding retention time and MS^n fragmentation profile data.

EGCG-rich extract				
Rt (min)	**Compound**	**$[M-H]^-$ (*m/z*)**	**MS^n product ions (*m/z*)**	**Ref.**
1.34	Gallic acid	169	MS^2: 169(100)	Co[a]
2.41	(epi)gallocatechin isomer	305	MS^2: 287(15), 261(40), 221(90), 219(100), 179(100), 165(35), 137(30), 125(35)	[18]
6.09	(epi)gallocatechin isomer	305	MS^2: 287(15), 261(40), 221(90), 219(95), 179(100), 165(30), 137(25), 125(30)	[18]
6.78	Catechin	289	MS^2: 245(100), 205(35), 203(20), 179(20)	Co
9.75	Epigallocatechingallate isomer	457	MS^2: 331(95), 305(45), 287(15), 269(10), 193(25), 169(100)	[18]
11.40	Epigallocatechingallate isomer	457	MS^2: 331(100), 305(50), 287(15), 269(10), 193(20), 169(90)	[18]
14.50	(epi)catechin gallate	441	MS^2: 331(20), 289(100)271(15), 193(10), 169(20)	[18]
PI extract				
Rt (min)	**Compound**	**$[M-H]^-$ (*m/z*)**	**MS^n product ions (*m/z*)**	**Ref.**
0.68	Quinic acid	191	MS^2: 173(30), 127(10), 111(100), 93(10), 85(40)	[19]
2.55	Protocatechuic acid	153	MS^2: 109(100)	Co
6.28	Protanthocyanidin B-type dimer	577	MS^2: 451(60), 425(100), 407(60), 289(50); MS^3[289]: 245 (100)	[20]
6.71	Protanthocyanidin B-type dimer	577	MS^2: 559(20), 441(20), 425(100), 407(60), 289(20); MS^3[289]: 245 (100)	[20]
6.79	Catechin	289	MS^2: 289(100), 205(40), 203(20), 179(20)	Co
7.32	Caffeic acid	179	MS^2: 135(100)	Co
12.99	Taxifolin-*O*-hexoside	465	MS^2:447(40), 437(70), 303(30), 285(100), 259(40); MS3[303]: 285(100), 177(15), 151(10), 125(10); MS3[285]: 257(25), 241(100), 217(55), 199(20), 175(40), 163(15)	
13.28	Taxifolin	303	MS^2: 285(100), 177(10); MS3[285]: 257(15), 241(100), 217(15), 199(25), 175(60)	[19]
RO extract				
Rt (min)	**Compound**	**$[M-H]^-$ (*m/z*)**	**MS^n product ions (*m/z*)**	**Ref.**
0.68	Quinic acid	191	173 (60), 129 (20), 127 (60), 111 (40), 93 (50), 85 (100)	[19]
2.44	Syringic acid	197	MS^2:179 (100), 135 (10)	[21]
7.47	Caffeic acid	179	161(10), 135(100)	Co
8.70	Chlorogenic acid	353	MS^2:191(20), 179(60), 173(100), 135(30)	Co
16.20	Luteolin-*O*-rutinoside isomer	593	MS^2: 285(100); MS^3[285]: 267(20), 241(80), 199(95), 175(100), 151(25)	[22]
16.88	Rosmarinic acid glucoside	521	MS^2: 359(100), 323(20)	[21]
17.04	Isorhamnetin-3-*O*-hexoside	477	MS^2: 462(10), 357(10), 315(100), 300(20); MS^3[315]:300(100)	[22]
18.18	Apigenin-7-*O*-glucoside	431	MS^2: 269(100), 268(20)	[22]
18.71	Rosmarinic acid	359	MS^2:223(10), 197(30), 179(30), 161(100)	[22]
19.42	Hesperetin-7-*O*-rutinoside	609	MS^2: 301(100), 285(20); MS^3[301]: 286(100), 283(60), 257(40), 242(80), 227(30), 215(20), 199(50), 125(20)	[22]
19.57	Luteolin-7-*O*-glucuronide	461	MS^2: 446(20), 299(30), 285(100); MS^3[285]: 267(40), 257(20), 241(100), 217(85), 199(90), 175(90), 151(40)	[22]
21.95	Luteolin-3-*O*-(2"-*O*-acetyl)-b-D-glucuronide isomer 1	503	MS^2: 285 (100); MS^3 [285]: 257(25), 241(100), 217(70), 199(100), 175(90), 151(60), 137 (15)	[19,21]
22.27	Luteolin-3-*O*-(2"-*O*-acetyl)-b-D-glucuronide isomer 2	503	MS^2: 443(10), 285 (100); MS^3 [285]: 257(30), 241(100), 217(80), 199(90), 175(80), 151(30)	[19,21]
22.79	Luteolin-*O*-rutinoside isomer	593	MS^2: 285(100); MS^3[285]: 267(100), 241(30), 240(40), 199(10), 185(50), 175(20)	[22]
24.44	Luteolin-3-*O*-(2"-*O*-acetyl)-b-D-glucuronide isomer 3	503	MS^2: 285 (100); MS^3 [285]: 257(30), 241(60), 217(100), 199(60), 175(80), 151(20)	[19,21]
24.38	Isorhamnetin-*O*-rutinoside	623	MS^2: 315(100), 300(70); MS^3 [315]: 300(100)	[22]
24.55	Luteolin-*O*-rutinoside isomer	593	MS^2: 285(100); MS^3[285]: 267(70), 257(80), 241(90), 199(100), 175(60), 151(50)	[22]
25.77	Apigenin	269	MS^2: 241(10), 227(20), 225(100), 201(30), 197(15), 181(20), 151(30)	[19]

[a] Identified by co-injection of standard

TABLE 2. Calibration data used for the quantification of phenolic compounds in EGCG-rich, PI and RO extracts.

Compound	λ (nm)	Conc. Range (µg/mL)	Calibration curve[a]	*R2*	LOD[b]	LOQ[b]
Gallic acid	280	5.2-62.4	*y* = -270843+159824*x*	0.9918	6.4	21.2
Catechin	280	5.1-61.2	*y* = -189194+46707*x*	0.9943	5.8	19.4
Caffeic acid	320	5.3-63.6	*y* = -372767+460017*x*	0.9927	6.1	20.4
Chlorogenic acid	280	5.8-19.4	*y* = -340173+96071*x*	0.9928	5.8	19.4
Luteolin	340	2.6-31.2	*y* = -393592+298270*x*	0.9943	2.7	8.9
Naringenin	280	5.1-51.0	*y* = -193351+390536*x*	0.9573	16.0	53.2
Isorhamnetin	340	4.4-44.0	*y* = -9218+220419*x*	0.9531	12.1	40.3

[a] *y* = peak area, *x* = concentration in µg/mL
[b] LOD – limit of detection, LOQ – limit of quantification, both expressed as µg/mL

TABLE 3. Phenolic compounds content in EGCG-rich, PI and RO extracts, expressed in mg/g of extract.

Rt	Compound	EGCG-rich	PI	RO
0.68	Quinic acid[a]	-	26.95 ± 0.92	7.46 ± 0.46
1.34	Gallic acid[a]	4.72 ± 0.33	-	-
2.44	Syringic acid[a]	-	-	2.19 ± 0.15
2.49	(Epi)gallocatechin isomer[b]	<LOQ	-	-
2.55	Protocatechuic acid[a]	-	1.81 ± 0.08	-
6.28	Proanthocyanidin B-typer dimer[b]	-	4.40 ± 0.40	-
6.46	(Epi)gallocatechin isomer[b]	16.75 ± 0.58	-	-
6.71	Proanthocyanidin B-typer dimer[b]	-	6.05 ± 0.44	-
7.06	Catechin[b]	8.46 ± 0.48	5.04 ± 0.35	-
7.47	Caffeic acid[c]	-	1.57 ± 0.09	1.55 ± 0.09
8.70	Chlorogenic acid[d]	-	-	<LOQ
9.84	(Epi)gallocatechin gallate isomer[b]	181.96 ± 6.73	-	-
11.19	(Epi)gallocatechin gallate isomer[b]	387.20 ± 15.53	-	-
12.99	Taxifolin-*O*-hexoside[e]	-	2.97 ± 0.06	-
13.28	Taxifolin[e]	-	1.20 ± 002	-
14.72	(Epi)catechin gallate[b]	36.22 ± 2.08	-	
16.20	Luteolin-*O*-rutinoside isomer[f]	-	-	1.64 ± 0.08
16.88	Rosmarinic acid glucoside[c]	-	-	2.82 ± 0.14
17.04	Isorhamnetin-3-*O*-hexoside[e]	-	-	2.32 ± 0.08
18.18	Apigenin-7-*O*-glucoside[f]	-	-	20.16 ±1.00
18.71	Rosmarinic acid[c]	-	-	3.50 ± 0.25
19.42	Hesperetin-7-*O*-rutinoside[g]	-	-	43.14 ± 1.09
19.57	Luteolin-7-*O*-glucuronide[f]	-	-	6.32 ± 0.15
21.95	Luteolin-3-*O*-(2”-*O*-acetyl)-b-D-glucuronide isomer[f]	-	-	4.59 ± 0.25
22.27	Luteolin-3-*O*-(2”-*O*-acetyl)-b-D-glucuronide isomer[f]	-	-	5.57 ± 0.18
22.79	Luteolin-*O*-rutinoside isomer[f]	-	-	2.66 ± 0.20
24.44	Luteolin-3-*O*-(2”-*O*-acetyl)-b-D-glucuronide isomer[f]	-	-	3.72 ± 0.25
24.55	Isorhamnetin-*O*-rutinoside[e]	-	-	1.31 ± 0.09
24.93	Luteolin-*O*-rutinoside isomer[f]	-	-	1.83 ± 0.06
25.77	Apigenin[f]	-	-	1.82 ± 0.10
	TOTAL	**635.31 ± 19.31**	**49.99 ± 0.82**	**112.59 ± 2.60**

Results correspond to the average±standard deviation estimated from the injection of three aliquots analyzed in triplicate
Calibrations curves used:
[a]Gallic acid, 280 nm
[b]Catechin acid, 280 nm
[c]Caffeic acid, 320 nm
[d]Chlorogenic acid, 280 nm
[e]Isorhamnetin, 340 nm
[f]Luteolin, 340 nm
[g]Naringenin, 280 nm

Hydrogels mineralization: dry mass percentage and ICP-OES analysis

GG hydrogels were prepared with the same mass of extract per unit mass of hydrogel to ensure addition of equal masses of extract (FIG. 1a). Hydrogel mineralization led, as expected, to increased opacity (FIG. 1b), due to the formation of CaP inside the hydrogel. Extract-free hydrogels were white. Hydrogels loaded with EGCG-rich extract were light pink. PI-loaded hydrogels were distinctly pink and RO-loaded hydrogels were yellow.

Dry mass percentage values (FIG. 1c) were markedly higher for hydrogels loaded with EGCG-rich extract. ICP-OES results (FIG. 1d) confirmed higher amounts of Ca and P in hydrogels loaded with EGCG-rich extract, indicating the highest level of mineralization for this group as the Ca:P ratio was markedly higher in this group.

The observed color development of the hydrogels suggests interactions between extract components and ALP, as was recently described for algae extracts in hydrogels [13]. Light and dark pink color development in GTE and in PI-loaded hydrogels (FIG. 1b) may be due to non-covalent interactions between ALP and EGCG in GTE, or between ALP and proanthocyanidins in PI, respectively. Interactions of proteins with polyphenols is a well described phenomenon and has also been observed, for example, for whey protein beta-lactoglobulin and EGCG [27,28]. In addition, anthocyanins are colorful pigments that alter between blue and red in dependence of the pH value [29], thus it is not necessarily an indicator for protein binding but rather the natural color of the pigments. The reasons for the development of the yellow color in RO-loaded hydrogels (FIG. 1b) remain unclear, although Bongartz et al. described that, depending on the pH value, the oxidation state and the type of interacting amino acid the color of a chlorogenic acid solution alters between green, red and yellow [30]. Similar mechanisms are possible for other phenolic acids such as rosmarinic acid. However, a detailed discussion is beyond the scope of this paper.

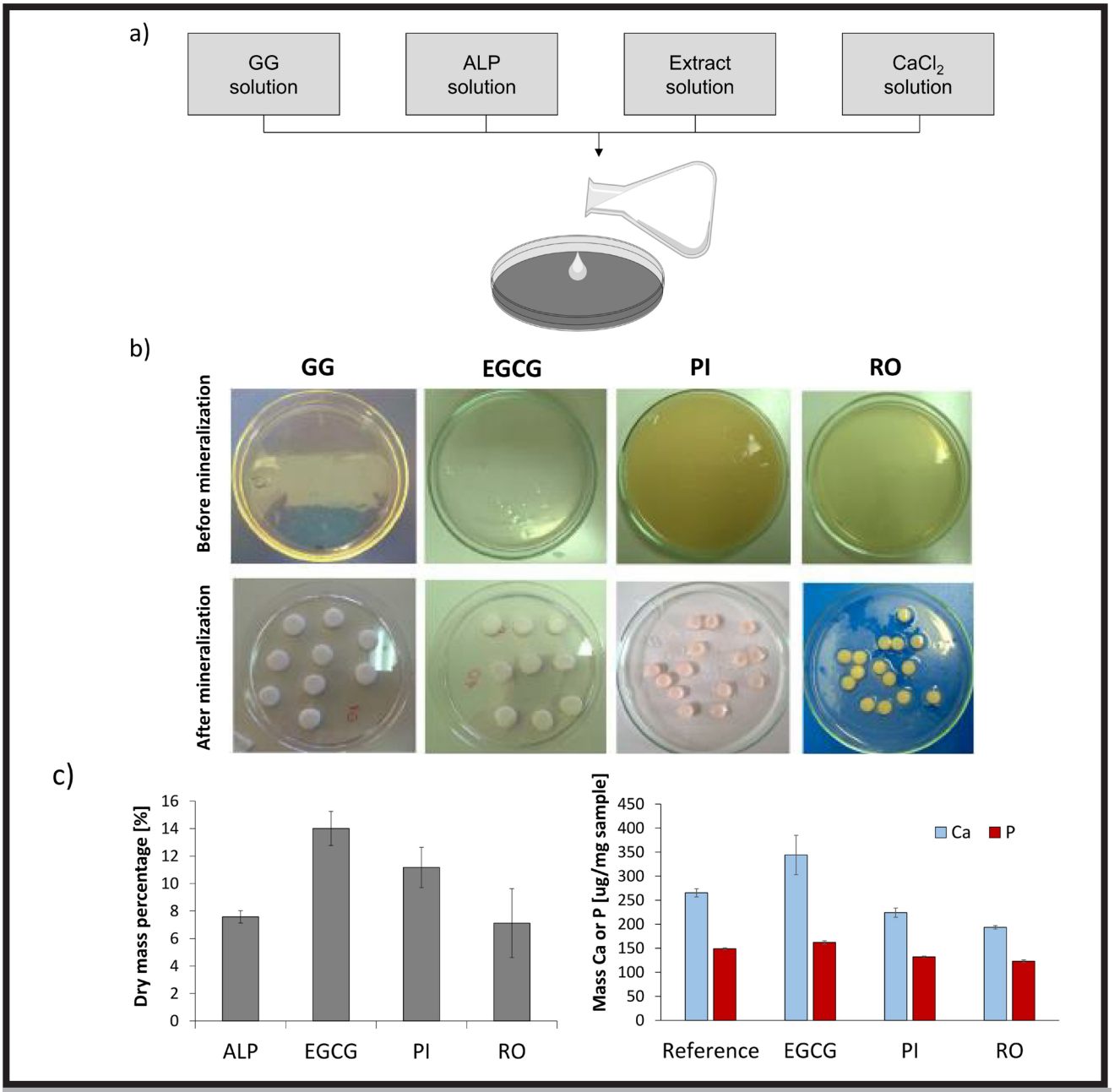

FIG. 1. (a) Method of production of extract-loaded GG hydrogels containing ALP; (b) Reference sample (GG) and samples with added extracts, *i.e.* EGCG-rich extract, PI and RO, before and after mineralization; (c) Dry mass percentage; (d) ICP-OES determination of mass of elemental Ca and P per unit mass hydrogel (µg/mg).

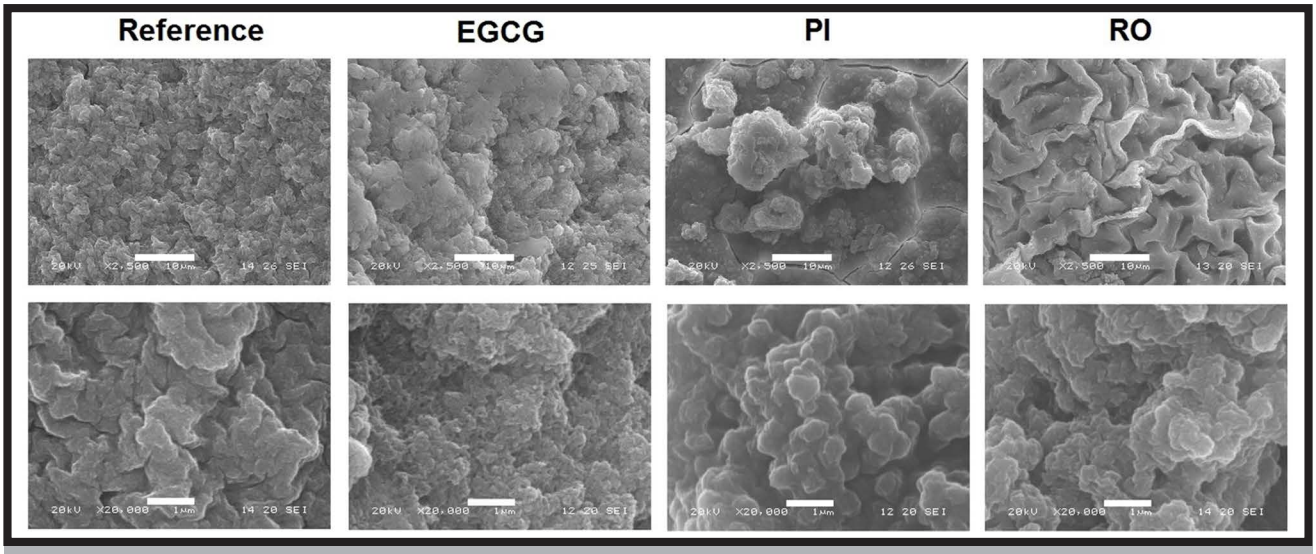

FIG. 2. SEM images of reference sample (GG) and samples with added extracts, i.e. EGCG-rich, PI and RO after mineralization. Top: magnification x2500. Bottom: magnification x20000. Scale bar: 10 μm (top), 1 μm (bottom).

The reasons why the EGCG-rich extract, promotes mineralization (FIG. 1c, 1d) may be hypothesized due to the binding of Ca^{2+} to EGCG, as EGCG has shown to form complexes with Ca^{2+} and proteins, which could stimulate CaP crystal nucleation [31]. Another possible explanation might be formation of complexes between polyphenols in the EGCG-rich extract and ALP, which could cause aggregation of ALP molecules or cause deformation leading to an increase in hydrodynamic diameter. Aggregation and increased hydrodynamic diameter would hinder ALP's diffusion from the hydrogel. This would increase intra-hydrogel ALP concentration, promoting CaP formation. The EGCG-rich extract contained a higher amount of phenolic compounds than the RO and PI extracts (TABLE 3). This may explain why the EGCG-rich extract promoted mineralization to a greater extent.

SEM and FTIR analysis

SEM microphotographs (FIG. 2) revealed a morphology consisting of mineral agglomerates on the surfaces of all mineralized hydrogels; thus, confirming their mineralization. The deposits were of sizes similar to those observed in GG hydrogels mineralized with ALP in previous works [32,33].

FTIR spectra (FIG. 3) confirmed mineralization by revealing bands characteristic for phosphate at 1100-1000 cm^{-1} (ν_3 stretching). Extract-loaded hydrogels exhibited a band at 870 cm^{-1}, corresponding to the ν_5 P–O(H) deformation of hydrogen phosphate groups, indicating formation of calcium-deficient hydroxyapatite (CDHA). In the case of EGCG-rich extract, the characteristic ν_3 stretching and ν_5 P–O(H) deformation bands were more pronounced. This finding and the higher Ca:P ratio in this group, suggest that the CDHA formed in the presence of this extract was of a higher degree of crystallinity. This outcome is consistent with previous work on enzymatic mineralization of catechol-PEG hydrogels [34], which revealed that presence of catechol groups displaying an affinity for Ca^{2+} ions and hydroxyapatite resulted in the highest degree of crystallinity [35,36].

The broad absorption band at approximately 3250 cm^{-1} indicated the presence of the O-H hydroxyl group, while the smaller bands at approximately 2900 and 2850 cm^{-1}, are due to C-H bending and the carboxyl -COOH group, respectively, while the bands at approximately 1675 cm^{-1} and 1040 cm^{-1} are due to the C-O carbonyl group from the glycosidic bond and the presence of a C-O-C ester group, respectively [37].

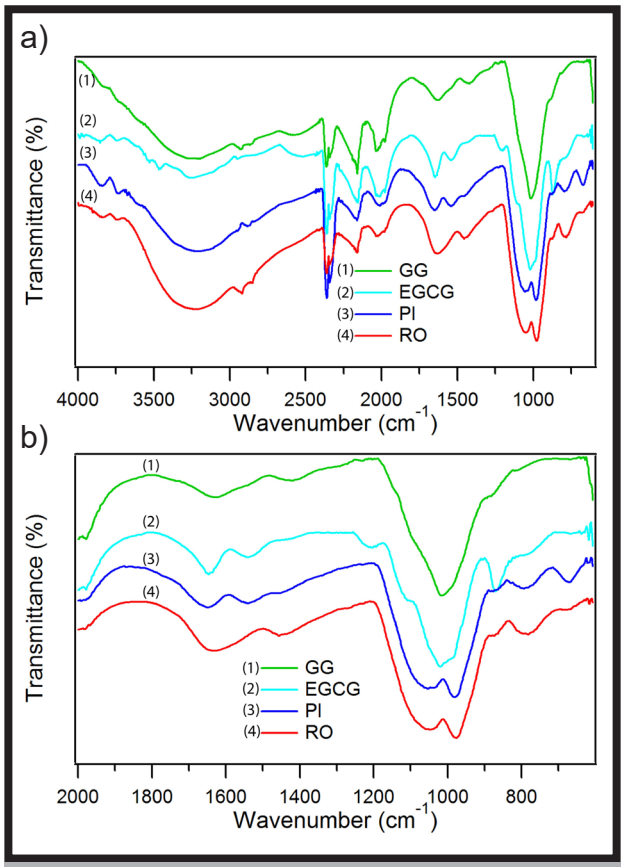

FIG. 3. FTIR spectra in the range 400-4000 cm^{-1} (a) and 400-2000 cm^{-1} (b) of reference GG hydrogels and GG hydrogels loaded with EGCG-rich, PI and RO extracts post-mineralization.

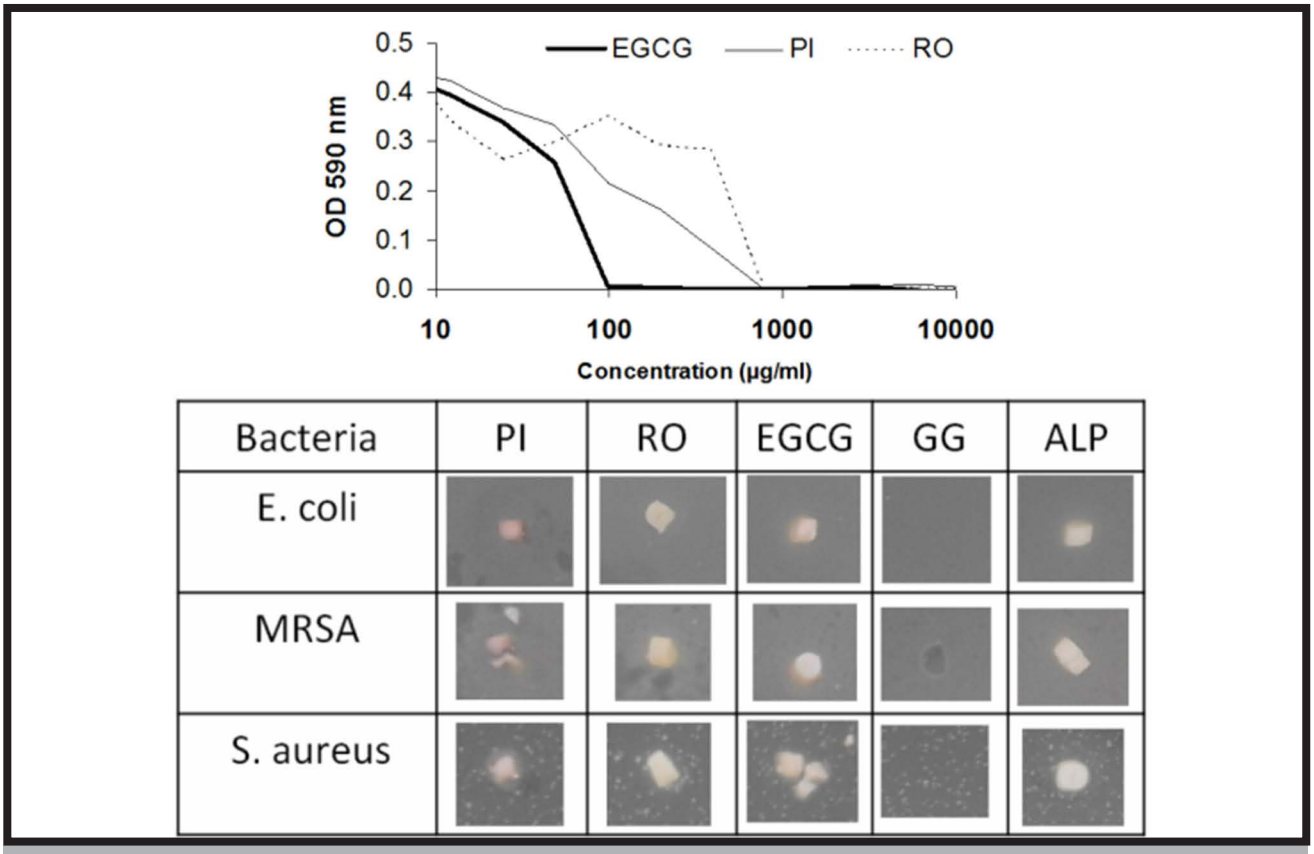

FIG. 4. Top: Minimal inhibitory concentration (MIC) of EGCG-rich, PI and RO extracts. Bottom: Representative images of the effect of the direct contact of the different hydrogels loaded with extracts post mineralization on growth of bacteria. GG: reference gellan gum hydrogel containing no extract or ALP. ALP: gellan gum hydrogel containing no extract.

Antibacterial properties

The minimal inhibitory concentration (MIC) test (FIG. 4) showed that all extracts, *per se*, lowered bacterial number, demonstrating antibacterial activity in the following order EGCG-rich > PI > RO.

The antibacterial activity in the order EGCG-rich > PI > RO (FIG. 4a) would be related with the higher quantity of phenolic compounds observed in EGCG-rich extracts, together with stronger antibacterial action of their components, namely EGC, catechin, EGCG and ECG (TABLE 1), which have been reported to be antibacterial towards *S. aureus* [38-40]. The PI extract displayed lower antibacterial activity. The polyphenols it contained (TABLE 1) have been reported to show different efficacies against *S. aureus*. Quinic acid, the major component found in PI extract, is reportedly ineffective against MRSA [41]. However, catechin, the B-type proanthocyanidin dimers or even other unidentified substances should be responsible for the antibacterial activity of this extract. RO extract displayed the lowest antibacterial activity against MRSA, although some of their components, such as apigenin derivatives and rosmarinic acid, have been reported to have considerable activity against *S. aureus* and MRSA [42].

Although solutions of the extracts themselves displayed antibacterial activity, antibacterial testing of extract-loaded hydrogels post-mineralization (FIG. 4) revealed that no zone of growth inhibition could be observed around any mineralized hydrogel discs, demonstrate lack of activity against any bacterial strain.

The lack of antibacterial activity of mineralized hydrogels (FIG. 4b) may be because bactericidal polyphenols and phenolic acids diffused out of the hydrogel during mineralization and/or become entrapped in the mineralized hydrogel. Hence the concentration of remaining polyphenols is below the MIC and hence too low to kill bacteria. Conceivably, a larger initial extract concentration should be used to guarantee antimicrobial activity after mineralization.

Further work will focus on cell biological characterization with bone-forming cells. It is believed that polyphenol-rich plant extracts will probably display minimal toxicity as they are used in traditional medicines but it is also believed that interactions of polyphenols with enzymes in eukaryotic cells is selective [9]. Therefore, in-depth testing is required.

Conclusion

In conclusion, EGCG-rich extract promoted hydrogel mineralization. EGCG-rich, PI and RO extracts all exhibited antibacterial activity against MRSA. Nevertheless, extract-loaded hydrogels post-mineralization did not appreciably hinder growth of MRSA, *E. coli* and *S. aureus.*

Acknowledgement

This work was supported by FWO, Belgium [postdoctoral fellowship: T.E.L.D.], BOF UGent, ERA-Net Rus project "Intelbiocomp" [A.G.S.], National Science Center, Poland (UMO-2018/29/N/ST8/01544), AgroForWealth: Biorefining of agricultural and forest by-products and wastes: integrated strategic for valorization of resources towards society wealth and sustainability (CENTRO-01-0145-FEDER-000001), funded by Centro2020, through FEDER and PT2020 and FCT (Fundação para a Ciência e Tecnologia) (financial support of CICECO-Aveiro Institute of Materials, and POCI-01-0145-FEDER-007679 (FCT UID/CTM/50011/2019)), and the N8 Agrifood Pump Priming Grant "Food2Bone", Lancaster University.

References

[1] E.M. Ahmed, Hydrogel: Preparation, characterization, and applications: A review. J Adv Res 6(2) (2015) 105-21.
[2] S. Donatan, A. Yashchenok, N. Khan, B. Parakhonskiy, M. Cocquyt, B.E. Pinchasik, D. Khalenkow, et al.: Loading Capacity versus Enzyme Activity in Anisotropic and Spherical Calcium Carbonate Microparticles. Acs Applied Materials & Interfaces 8(22) (2016) 14284-14292.
[3] M. Maitra, V.K. Shukla: Cross-linking in Hydrogels - A Review. Am J Polym Sci 4(2) (2014) 25.
[4] D.F. Coutinho, S.V. Sant, H. Shin, J.T. Oliveira, M.E. Gomes, N.M. Neves, A. Khademhosseini, R.L. Reis: Modified Gellan Gum hydrogels with tunable physical and mechanical properties, Biomaterials 31(29) (2010) 7494-502.
[5] C.J. Ferris, K.J. Gilmore, G.G. Wallace, M.i.h. Panhuis: Modified gellan gum hydrogels for tissue engineering applications, Soft Matter 9(14) (2013) 3705-3711.
[6] T.E. Douglas, A. Dokupil, K. Reczynska, G. Brackman, M. Krok-Borkowicz, J.K. Keppler, M. Bozic, P. Van Der Voort, K. Pietryga, S.K. Samal, L. Balcaen, J. van den Bulcke, J. Van Acker, et al.: Enrichment of enzymatically mineralized gellan gum hydrogels with phlorotannin-rich Ecklonia cava extract Seanol((R)) to endow antibacterial properties and promote mineralization, Biomed Mater 11(4) (2016) 045015.
[7] J.R. Mediavilla, L. Chen, B. Mathema, B.N. Kreiswirth: Global epidemiology of community-associated methicillin resistant Staphylococcus aureus (CA-MRSA), Curr Opin Microbiol 15(5) (2012) 588-95.
[8] A.C. Uhlemann, M. Otto, F.D. Lowy, F.R. DeLeo: Evolution of community- and healthcare-associated methicillin-resistant Staphylococcus aureus, Infect Genet Evol 21 (2014) 563-74.
[9] T.P.T. Cushnie, A.J. Lamb: Antimicrobial activity of flavonoids, International Journal of Antimicrobial Agents 26(5) (2005) 343-356.
[10] A.N. Panche, A.D. Diwan, S.R. Chandra: Flavonoids: an overview, J Nutr Sci 5 (2016) e47.
[11] S. Swioklo, K.A. Watson, E.M. Williamson, J.A. Farrimond, S.E. Putnam, K.A. Bicknell: Defining Key Structural Determinants for the Pro-osteogenic Activity of Flavonoids, J Nat Prod 78(11) (2015) 2598-2608.
[12] Y. Yoda, Z.Q. Hu, W.H. Zhao, T. Shimamura: Different susceptibilities of Staphylococcus and Gram-negative rods to epigallocatechin gallate, J Infect Chemother 10(1) (2004) 55-8.
[13] E. Hames-Kocabas, O. Yesil-Celiktas, M. Isleten, F. Vardar-Sukan: Antimicrobial activity of pine bark extract and asssessment of potential application in cooked red meat, GIDA 33(3) (2008) 123-127.
[14] S. Moreno, T. Scheyer, C.S. Romano, A.A. Vojnov: Antioxidant and antimicrobial activities of rosemary extracts linked to their polyphenol composition, Free Radical Research 40(2) (2006) 223-231.
[15] R. Touati, S.A.O. Santos, S.M. Rocha, K. Belhamel, A.J.D. Silvestre: Phenolic composition and biological prospecting of grains and stems of Retama sphaerocarpa, Industrial Crops and Products 95 (2017) 244-255.
[16] T.E. Douglas, A. Lapa, K. Reczynska, M. Krok-Borkowicz, K. Pietryga, S.K. Samal, H.A. Declercq, D. Schaubroeck, M. Boone, P. Van der Voort, K. De Schamphelaere, C.V. Stevens, V. Bliznuk, L. Balcaen, B.V. Parakhonskiy, F. Vanhaecke, V. Cnudde, E. Pamula, A.G. Skirtach: Novel injectable, self-gelling hydrogel-microparticle composites for bone regeneration consisting of gellan gum and calcium and magnesium carbonate microparticles, Biomed Mater 11(6) (2016) 065011.
[17] A.W. Bauer, W.M. Kirby, J.C. Sherris, M. Turck: Antibiotic susceptibility testing by a standardized single disk method, Tech Bull Regist Med Technol 36(3) (1966) 49-52.
[18] D. Del Rio, A.J. Stewart, W. Mullen, J. Burns, M.E. Lean, F. Brighenti, A. Crozier: HPLC-MSn analysis of phenolic compounds and purine alkaloids in green and black tea, Journal of agricultural and food chemistry 52(10) (2004) 2807-2815.
[19] R. Touati, S.A. Santos, S.M. Rocha, K. Belhamel, A.J. Silvestre: Phenolic composition and biological prospecting of grains and stems of Retama sphaerocarpa, Industrial crops and products 95 (2017) 244-255.
[20] M. de la Luz Cádiz-Gurrea, S. Fernández-Arroyo, A. Segura-Carretero: Pine bark and green tea concentrated extracts: antioxidant activity and comprehensive characterization of bioactive compounds by HPLC–ESI-QTOF-MS, International journal of molecular sciences 15(11) (2014) 20382-20402.
[21] M. Achour, R. Mateos, M. Ben Fredj, A. Mtiraoui, L. Bravo, S. Saguem: A comprehensive characterisation of rosemary tea obtained from Rosmarinus officinalis L. collected in a sub-humid area of Tunisia, Phytochemical analysis 29(1) (2018) 87-100.
[22] P. Mena, M. Cirlini, M. Tassotti, K.A. Herrlinger, C. Dall'Asta, D. Del Rio: Phytochemical Profiling of Flavonoids, Phenolic Acids, Terpenoids, and Volatile Fraction of a Rosemary (Rosmarinus officinalis L.) Extract, Molecules 21(11) (2016).
[23] D. Del Rio, A.J. Stewart, W. Mullen, J. Burns, M.E. Lean, F. Brighenti, A. Crozier: HPLC-MSn analysis of phenolic compounds and purine alkaloids in green and black tea, J Agric Food Chem 52(10) (2004) 2807-15.
[24] H.A. Weber, A.E. Hodges, J.R. Guthrie, B.M. O'Brien, D. Robaugh, A.P. Clark, R.K. Harris, J.W. Algaier, C.S. Smith: Comparison of proanthocyanidins in commercial antioxidants: grape seed and pine bark extracts, J Agric Food Chem 55(1) (2007) 148-56.
[25] S. Iravani, B. Zolfaghari: Pharmaceutical and nutraceutical effects of Pinus pinaster bark extract, Res Pharm Sci 6(1) (2011) 1-11.
[26] E.N. Frankel, S.W. Huang, R. Aeschbach, E. Prior: Antioxidant activity of a rosemary extract and its constituents, carnosic acid, carnosol, and rosmarinic acid, in bulk oil and oil-in-water emulsion, Journal of Agricultural and Food Chemistry 44(1) (1996) 131-135.
[27] J.K. Keppler, D. Martin, V.M. Garamus, K. Schwarz: Differences in binding behavior of (-)-epigallocatechin gallate to -lactoglobulin heterodimers (AB) compared to homodimers (A) and (B), Journal of Molecular Recognition 28(11) (2015) 656-666.
[28] S. Wiese, S. Gartner, H.M. Rawel, P. Winterhalter, S.E. Kulling: Protein interactions with cyanidin-3-glucoside and its influence on alpha-amylase activity, Journal of the Science of Food and Agriculture 89(1) (2009) 33-40.
[29] H.E. Khoo, A. Azlan, S.T. Tang, S.M. Lim: Anthocyanidins and anthocyanins: colored pigments as food, pharmaceutical ingredients, and the potential health benefits, Food & Nutrition Research 61 (2017) 1-21.
[30] V. Bongartz, L. Brandt, M.L. Gehrmann, B.F. Zimmermann, N. Schulze-Kaysers, A. Schieber: Evidence for the Formation of Benzacridine Derivatives in Alkaline-Treated Sunflower Meal and Model Solutions, Molecules 21(1) (2016).
[31] F. Fuchs, Z. Grabarek: The green tea polyphenol (-)-epigallocatechin-3-gallate inhibits magnesium binding to the C-domain of cardiac troponin C, Journal of Muscle Research and Cell Motility 34(2) (2013) 107-113.
[32] T.E. Douglas, G. Krawczyk, E. Pamula, H.A. Declercq, D. Schaubroeck, M.M. Bucko, L. Balcaen, P. Van Der Voort, V. Bliznuk, N.M. van den Vreken, M. Dash, et al.: Generation of composites for bone tissue-engineering applications consisting of gellan gum hydrogels mineralized with calcium and magnesium phosphate phases by enzymatic means, J Tissue Eng Regen Med 10(11) (2016) 938-954.
[33] T.E.L. Douglas, M. Pilarz, M. Lopez-Heredia, G. Brackman, D. Schaubroeck, L. Balcaen, V. Bliznuk, P. Dubruel, C. Knabe-Ducheyne, F. Vanhaecke, T. Coenye, E. Pamula: Composites of gellan gum hydrogel enzymatically mineralized with calcium-zinc phosphate for bone regeneration with antibacterial activity, J Tissue Eng Regen Med 11(5) (2017) 1610-1618.
[34] T.E. Douglas, P.B. Messersmith, S. Chasan, A.G. Mikos, E.L. de Mulder, G. Dickson, D. Schaubroeck, L. Balcaen, F. Vanhaecke, P. Dubruel, J.A. Jansen, S.C. Leeuwenburgh: Enzymatic mineralization of hydrogels for bone tissue engineering by incorporation of alkaline phosphatase, Macromol Biosci 12(8) (2012) 1077-89.
[35] W.M. Chirdon, W.J. O'Brien, R.E. Robertson: Adsorption of catechol and comparative solutes on hydroxyapatite, J Biomed Mater Res B Appl Biomater 66(2) (2003) 532-8.
[36] J. Ryu, S.H. Ku, H. Lee, C.B. Park: Mussel-Inspired Polydopamine Coating as a Universal Route to Hydroxyapatite Crystallization, Adv. Funct. Mater. 20 (2010) 2132–2139.
[37] A.M. Jaafar, V .Thatchinamoorthi, Preparation and Characterisation of Gellan Gum Hydrogel containing Curcumin and Limonene, IOP Conf. Series: Materials Science and Engineering 440 (2018) 012023
[38] T.O. Ajiboye, M. Aliyu, I. Isiaka, F.Z. Haliru, O.B. Ibitoye, J.N. Uwazie, H.F. Muritala, S.A. Bello, I.I. Yusuf, A.O. Mohammed: Contribution of reactive oxygen species to (+)-catechin-mediated bacterial lethality, Chemico-Biological Interactions 258 (2016) 276-287.
[39] J.C. Anderson, R.A. McCarthy, S. Paulin, P.W. Taylor: Anti-staphylococcal activity and beta-lactam resistance attenuating capacity of structural analogues of (-)-epicatechin gallate, Bioorg Med Chem Lett 21(23) (2011) 6996-7000.
[40] B.S. Fazly Bazzaz, S. Sarabandi, B. Khameneh, H. Hosseinzadeh: Effect of Catechins, Green tea Extract and Methylxanthines in Combination with Gentamicin Against Staphylococcus aureus and Pseudomonas aeruginosa: - Combination therapy against resistant bacteria, J Pharmacopuncture 19(4) (2016) 312-318.
[41] C.O. Rezende, L.A. Oliveira, B. Oliveira, C.G. Almeida, B.S. Ferreira, M. Le Hyaric, G.S.L. Carvalho, M.C.S. Lourenco, M. Batista, F.K. Marchini, et al: Synthesis and Antibacterial Activity of Alkylated Diamines and Amphiphilic Amides of Quinic Acid Derivatives, Chemical Biology & Drug Design 86(3) (2015) 344-350.
[42] S.P. Ekambaram, S.S. Perumal, A. Balakrishnan, N. Marappan, S.S. Gajendran, V. Viswanathan: Antibacterial synergy between rosmarinic acid and antibiotics against methicillin-resistant Staphylococcus aureus, Journal of Intercultural Ethnopharmacology 5(4) (2016) 358-363.

ELECTROSPINNING FOR DRUG DELIVERY SYSTEMS: POTENTIAL OF THE TECHNIQUE

Ewa Dzierzkowska*, Ewa Stodolak-Zych

AGH University of Science and Technology,
Faculty of Materials Science and Ceramics,
al. A. Mickiewicza 30, 30-059 Kraków, Poland
*e-mail: dzierzkowska@agh.edu.pl

Abstract

Electrospinning is a technique used to manufacture nano- and submicron fibers based on synthetic or natural polymers. Additionally, biomaterials used in the electrospinning procedure can be modified by bioactive compounds, e.g. peptides or growth factors. The microstructure of the obtained fibrous scaffolds mimics natural extracellular matrix (ECM) environment. The size and the microstructure of the fibrous scaffolds are considered to be suitable for cells adhesion and proliferation.

Various design features of the electrospinning device (e.g. the shape of the collector, the shape of the nozzle, the direction of the applied voltage) or electrospinning conditions (e.g. humidity, temperature) allows to control properties of the fibers (their shape, diameter, porosity). Novel structures, such as core-shell fibers, porous fibers attracted wide attention due to their properties and functionalities. Porous fibers or fibers with nanoscaled structures can be obtained in several ways. These methods are mainly focused on using high humidity and highly volatile solvent applied in the electrospinning process. The core-shell structure can be obtained by coaxial electrospinning. That binary fiber has ability to control the release rate of drug enclosed within the shell or core. The drug release profile can be also modified by loading the pharmacological agent either directly to the spinning solution or its post immobilization.

This diversity of the electrospun fibers is a reason for non-woven materials to be considered for application as drug carriers. The review of electrospinning methods presented here proves that the control over fibers surface area, morphology and the choice of polymer enable modelling of drug release kinetics.

Keywords: *electrospinning, drug carrier, DDS, nanofibers, polymer*

[Engineering of Biomaterials 149 (2019) 10-14]

Introduction

The main challenge in designing drug carriers is an effective biodistribution of the pharmacological agents in the body. Thus, the form of a carrier plays an important role in the drug release process. There are many types of carriers such as micelles, microcapsules, microspheres, liposomes, proteins, and DNA. Lately, scientists have been paying particularly great attention to (nano)fibers. Such form of the material can be obtained by several techniques like template synthesis, self-assembly, phase separation method, airbrush spray, melt blow technology, and the most popular one – electrospinning. In the last one, the polymeric solution is transformed into solid fibers by application of electrical force [1]. There are numerous critical factors, including process parameters, solution parameter, and ambient parameters, that have an influence on the morphology of the fibers and the whole membrane. These variables determine fibers morphology which, in consequence, affects the drug release profile. The electrospun mats have fiber diameter ranging from several dozen of nanometers to microns. These materials are characterized by high porosity and high surface area to volume ratio which allow efficient drug loading. It is also possible to create porosity within a single fiber. That can further enhance surface development and increase the functionality of the fibers. Furthermore, the drug release can be controlled by loading the pharmacological agent either directly to the spinning solution or by its post-immobilization. There are also other techniques for drug incorporation. In the case of less stable drugs, use of emulsion electrospinning or co-axial strategies is recommended.

This review summarizes current possibilities of producing fibrous drug carriers.

Parameters determining the properties of the fibers

A typical electrospinning setup consists of 3 main components: high voltage power supply, syringe pump with attached metal nozzle (needle) and grounded collector (metal shield, plate, rotating drum). The polymer solution is introduced via a syringe pump. When a high voltage (typically 1-30 kV) appears between the metal nozzle and the collector, the polymer solution inside the syringe becomes electrically charged. When the electrostatic force is greater than the surface tension of the polymer drop at the end of the metal nozzle, the droplet is pulled out of the needle. The shape of the drop resembles a cone, known as the Taylor's cone. The thin stream of fiber is accelerated to the collector with opposite polarity. During the passage of the fiber stream from the needle to the collector, the solvent present in the polymer solution evaporates allowing the polymer fiber to solidify on the collector [2-4].

A number of processing parameters can be adopted to obtain the desired diameter and morphology of the nanofibers. They can be divided into three groups: process, polymer, and ambient parameters. Process parameters include applied voltage, the flow rate of the solution, the distance between the tip of the needle and the collector and the type of the collector [5]. The most common collector design is the single static plate collector. The plate can be changed to the rotating drum. This modification allows to obtain parallel fibers by increasing the rotation speed of the drum. Dual collectors can be obtained as well when a gap is left between them. As a result, the electrospun fibers are suspended in the air. A similar solution can be found in a ring collector, which has an empty interior. It is also possible to co-electrospun fibers onto a rotating collector (two separate syringe pumps and nozzles sets are needed) or electrospray and electrospun simultaneously. These numerous permutations of the collector design have an effect on the final morphology of the fibers [6]. The rest of the process parameters affect mainly fibers diameter. Increase in applied voltage causes a decrease in fibers diameter. The same effect is observed when increasing distance between the needle and the collector or decreasing the flow rate [5] (TABLE 1).

TABLE 1. Effects of electrospinning prameters on fibers microstucture.

Paramters	Effect on the fiber morphology
Supplied voltage	↑voltage ↓fiber diameter
Flow rate	↓flow rate ↓fiber diameter
Distance between needle and the collector	↑distance ↓fiber diameter
Polymer concentration	↑concentration ↑fiber diameter
Polymer viscosity	↑viscosity ↑fiber diameter
Polymer molar mass	↓molar mass provides bead formation
Solvent volatility	↑volatility – porous fiber ↓volatility – fibers stick together on the collector
Solution conductivity	↑conductivity – homogeneous fibers diameters
Temperature	↑temperature ↓fiber diameter
Humidity	↑humidity ↓fiber diameter

Also, polymer solution parameters, such as polymer concentration, solution viscosity, the molar mass of polymer, solvent volatility and solution conductivity have an impact on the electrospinning process. Spinnability of the solution is the most important factor which is determined by the polymer concentration. It has to be high enough to allow forming fibers. On the other hand, too high concentration and viscosity impedes passing of the solution through the needle and may cause dropping of the solution from the needle prior to the actual electrospinning process. A highly concentrated solution results in a greater number of entangled polymer chains, which translates into a larger fiber diameter of uniform thickness. At gradually lower polymer concentrations, the resulting fibers become thinner and may contain a large number of beads. Too low concentration and too low viscosity cause lack of spinning or interruption of the beam and the formation of droplets. In this way, the electrospinning process can transform into electrospray. Thus, there are critical concentration and viscosity values at which the concentration of polymer chains entanglements allows the formation of a continuous polymeric stream. It is worth underlining that by increasing these two parameters, the diameter of the resulting fibers may be increased. A suitable viscosity of a polymer solution is provided by a molar mass. Lower molar mass leads to the formation of beads. The role of a solvent is not only to dissolve a polymer but also to transfer the polymer solution towards the collector. Solvent parameters like surface tension, conductivity and vapour pressure are of equal importance. Low vapour pressure and thus high volatility are desirable properties of the solvent. As a result, the entire solvent evaporates completely when the jet is transferred to the collector. When using a solvent with low volatility, the fibers on the collector stick together or flatten. The increased volatility of the solvent also gives a greater chance of producing porous single fibers. All these parameters have an influence on a solution surface tension, which determines the amount of charge needed to initiate the jet. With a smaller surface tension, a low value of voltage created by the power supply to remove the drop from the needle is needed. In the case of high surface tension, the electrospinning process is more difficult [5,7-9].

The ambient parameters are also very relevant. The thickness of the fibers can be controlled by temperature and humidity. The increase in temperature is associated with a reduction in fiber diameter. This is due to the drop in polymer viscosity at elevated temperature. Humidity affects the electrical conductivity of the ambient atmosphere/air. The increase in humidity causes the tensile forces to be more efficient, facilitating the spinning of the fibers from solutions of high viscosity, and the applied voltage can be significantly lower. Lower humidity results in rapid evaporation of the solvent, resulting in thicker fibers, while higher values cause slower evaporation of the solvent resulting in thinner fibers. Changes in humidity and/or higher temperature may contribute to the formation of pores on fiber surfaces, as these parameters affect the evaporation rate of the solvent [5].

Drug incorporation method

The specific form of fiber provides several options for drug incorporation. The basic approach is blend electrospinning (FIG. 1C). Drug and polymer are co-dissolved in solvents before electrospinning process. In the case of this method, the crucial factor is a proper distribution of the drug in the entire volume of a solution. Preferably, active agents should be evenly distributed within the final electrospun fibers. In practice, most molecules, during the electrospinning process, migrate to the surface of the solidifying fibers due to evaporation of the solvent. The molecules of the drug deposited on the fiber surface can be readily released, causing an undesirable burst effect. It is also worth mentioning that appropriate selection of a solvent, polymer and drug system is challenging for blend electrospinning [4].

This limitation can be overcome by applying emulsion electrospinning (FIG. 1B). This technique is based on two immiscible liquids stabilized by an emulsifier. In this way, biomolecules or hydrophilic drugs are protected from a solvent used in a polymer solution. During the electrospinning process, the obtained droplets may be distributed homogeneously within fibers, locate close to the surface or form a core-shell structure. The core-shell structures are obtained when solvent from the outer part of a polymer jet, the surface, evaporates faster than from the inner part. The viscosity of the surface is much higher compared to the interior. Then, emulsion droplets are induced to move from the outside to the inside of the polymer jet. Under a high-voltage conditions, emulsion droplets are stretched and condensed along the fibers axis. Optimal parameters ensure that a fibrous core-shell structure is obtained without using a specific nozzle. Furthermore, emulsion electrospinning allows the encapsulation of less stable molecules and provides a sustained drug release without burst effect [10].

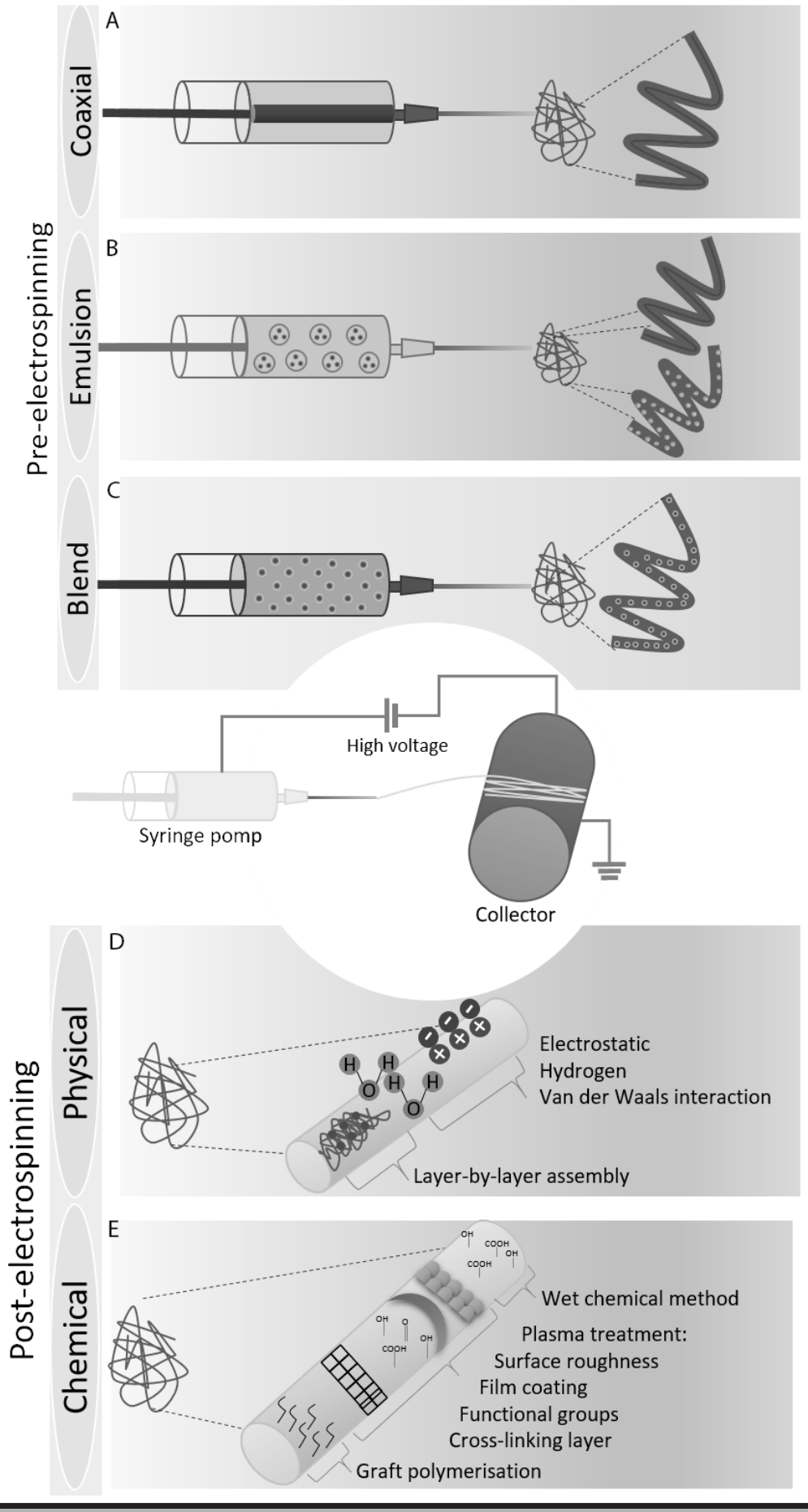

FIG. 1. Strategies of incorporating drug: A - co-axial electrospinning; B - emulsion electrospinning; C - blend electrospinning; D - physical surface modification; E - chemical surface modification.

The core-shell structure can also be manufactured in an intended manner using co-axial electrospinning (FIG. 1A). This strategy is based on simultaneous electrospinning of two kinds of immiscible polymer solutions through two concentrating nozzles. Use of two different solutions increases the difficulty of optimizing process parameters. It is also possible to generate empty space inside the fibers by removing the internal phase of the core. This technique can be used to encapsulate unstable macromolecules [4,6].

The possibility of introducing active molecules into the fibers prior to the electrospinning process is not the only way to combine the drug with a fiber. Active molecules can also be adsorbed onto a surface of the fibers as a result of physical (FIG. 1D) or chemical interactions (FIG. 1E). Simple adsorption is an example of a physical post-immobilization. It is a common method of applying a drug onto a fibrous membrane. Adsorption of molecules onto the fibers is driven by electrostatic interactions, hydrogen bonds, and van der Waals interactions. The fibrous membranes have a higher surface to volume ratio, as a result of which a larger amount of drug can be deposited onto the surface of the fiber than introduced into their volume. For that reason, the immediate release of a very high dose of an active substance may be observed. A similar surface functionalization process takes place in the case of nanoparticles. The method of the physical surface modification can be also realized by a multilayer assembly. The method is based on applying layers of polyanions and polycations to the charged surface by electrostatic forces [4].

Another approach is to modify fibers surface chemically, which causes the formation of reactive functional groups. Such transformation of surface groups allows the immobilization of molecules with covalent bonds. This results in a stronger attachment of a molecule compared to the physical adsorption. As a result, the drug introduced into the fibers remains attached to it for a long time. An example of chemical modification is a plasma treatment. Commonly, plasma is used to optimize wetting properties and adapt adhesion of the surface by changing the surface chemical composition. Polymer surface can be modified by adding different functional groups to improve the biocompatibility [11]. Formation of carboxyl groups or amine groups on the surface of the fibers through plasma treatment with air, oxygen or ammonia, causes immobilization of ECM components on their surface, such as collagen, gelatin, laminin, and fibronectin. This process enhances cell adhesion and proliferation [12]. Moreover, plasma treatment can be also used to coat a surface with a thin film, tailor surface roughness or to induce crosslink formation and graft polymerization. Plasma treatment has also some limitations [11]. Most importantly, only the very surface of the fibrous membrane can be modified due to restricted plasma depth penetration. Other chemical post-mobilization methods which can overcome this restriction is a wet chemical method, based on surface hydrolysis. Surface hydrolysis leads to cleavage of ester bonds in polymer chains. As a result, carboxylic and hydroxyl groups are formed on the surface from degraded, but insoluble, polymer fragments. Plasma treatment and UV radiation cause the formation of free radicals for polymerization on the surface of the fibrous membrane. This operation makes the surface hydrophilic and allows the connection of active agents to a membrane by covalent bonding [12].

Factors affecting drug release

Release of drugs from fibers can be affected by desorption, dissolving, diffusion through water-filled pores and degradation of a polymer matrix. Therefore, the direct factor that affects the release of the drug from the fibers was discussed in the previous paragraph. Blend electrospinning provides drug release through diffusion and degradation of the polymer. This model is characterized by the immediate release of the entire active factor from the fibers. Sustained release with initial burst effect is represented in the case of surface functionalized fibers through diffusion model. Here, the release rate is influenced by the attachment strength of the molecules. The most sustained drug release can be obtained from core-shell or emulsified structures, caused by the degradation of the shell [13,14]. For molecules introduced into the fibers, their diameter has a key role in drug release rate. Thinner fibers have a high surface area to volume ratio that provides larger surfaces for mass exchange and results in a faster release [8]. Also, the distance between a surface and a core of fibers from where active molecules are dissolved is very small [3]. Increasing the contact surface can be achieved by producing porous fibers. Thus, the thicker fibers with high porosity are characterized by faster release when compared to thinner fibers but without pores. Membrane porosity, and hence the orientation of the fibers, also determines the drug release rate. It will be lower in the case of a membrane with parallel, closely arranged fibers than randomly distributed [8]. Moreover, physicochemical drug properties (hydrophilic, hydrophobic), the interaction between a drug and a polymer matrix, molecular weight of a polymer, and degradation rate of a polymer matrix can influence the drug release profile. Polymer degradation is related to its crystallinity. The polymers with amorphous structure degrade faster, providing a faster release of the drug from the matrix. The higher degree of crystallinity, the slower the degradation and the release of the drug. What is more, the degradation depends on the hydrophilic/hydrophobic surface character. The more hydrophilic material, the better water penetration and the faster degradation and desorption of the drug. Hydrophobic material swells in the aqueous environment, releasing small doses of the drug over a long period of time. Combining the drug with the matrix by covalent bond results in sustained release or sustained release with the burst effect in the first days. On the other hand, second-order interactions (hydrogen, van der Waals) ensure the immediate release of the drug [13].

Formation of porous fibers

The electrospun membranes are characterized by high surface area. This property can be further increased by producing porous fibers. Careful solvent selection and appropriate ambient conditions allow to achieve surface or internal porosity. This unique microstructure may be observed as wrinkles, nanopores, porous or hollow interiors. Two mechanisms can explain pore formation in polymer fibers, i.e. based on phase separation or breath figures. By selecting volatile solvents that are immiscible with water and have low dielectric constants, the pores are obtained using the breath figures mechanism. During electrospinning process in a humid environment (above 50%) evaporation of volatile molecules of solvents, causes a decrease in the temperature on the surface of the fiber. As a result of high humidity, water vapor droplets condensate on the fibers. Those droplets leave circular imprints and pores of the same shape are formed after water evaporation from the surface.

In the case of phase separation, a rich polymer phase and the poor one are formed when a polymer solution becomes thermodynamically unstable. The pores are represented by a polymer-poor phase. Three phase separation methods resulting in pore formation have been identified. Firstly, thermally induced phase separation (TIPS) based on a dynamic change of temperature. The decrease of the temperature leads to evaporation of the volatile solvent from the homogeneous solution. Another phase separation mechanism is vapour induced phase separation (VIPS). Water vapour droplets from a humid environment are attracted to the surface of the electrospun jet and penetrate it. The water vapour droplets mix with the solvent and become a non-solvent for the polymer, inducing phase separation. After complete evaporation of the water-solvent solution, highly porous structures are obtained. VIPS, TIPS, and breath figures are mechanisms which explain the formation of the porous fibers in a single solvent system. In the ternary system consisting of two solvents with one non-solvent, a non-solvent induced phase separation (NIPS) takes place. There are also other methods for obtaining porous fibers, like eg. using polymer blends and subsequent removing of one of the components, use of bath collector or appropriate additives, etc. However, there are a few limitations of these methods. Namely, need for: post-treatment of the electrospun membrane, modification of the device, or the optimization of an effect of introduced additives on the properties of the fibers [21,22].

Conclusions

Electrospinning is a simple technique for the manufacturing of nano- and submicrofibers characterized by high porosity and high surface area to volume ratio. These properties of electrospun nanofibers have been highly exploited in biomedical applications such as tissue engineering, regenerative medicine, wound dressing, enzyme immobilization and recently in drug delivery. Manufacturing of the electrospun fibers depends significantly on various parameters: solution parameters, equipment parameters, and ambient parameters. Optimization of these parameters is crucial for obtaining electrospun nanofibers with desirable properties. In the field of drug delivery, different electrospinning methods such as direct method and coaxial electrospinning have been successfully used for fabrication of nanofibers with various drug release behaviour including fast, biphasic, delayed or controlled release. The physical and chemical stability of these polymer-drug fibers systems is a very complex phenomenon, hence the drug release kinetics have not been thoroughly explored yet. Nevertheless, the various possibilities offered by electrospun nanofibers in drug delivery systems guarantee rapid development of this technique for biomedical applications.

Acknowledgments

This work was performed within the framework of funding for statutory activities of AGH University of Science and Technology in Krakow, Faculty of Materials Science and Ceramics (11.11.160.182).

References

[1] Kamble P., Sadarani B., Majumdar A., Bhullar S.: Nanofiber based drug delivery systems for skin: A promising therapeutic approach. J. Drug Deliv. Sci. Technol. 41 (2017) 124-133.
[2] Jiang T., Carbone E.J., Lo K. W.-H., Laurencin C.T.: Electrospinning of polymer nanofibers for tissue regeneration. Prog. Polym. Sci. 46 (2015) 1-24.
[3] Thakkar S., Misra M.: Electrospun polymeric nanofibers: New horizons in drug delivery. Eur. J. Pharm. Sci. 107 (2017) 148-167.
[4] Wang J. Windbergs M.: Functional electrospun fibers for the treatment of human skin wounds. Eur. J. Pharm. Biopharm. 119 (2017) 283-299.
[5] Bang C.Z.: Electrospinning PLA/PEO/HNTs membranes loaded with 5-Fluorouracil for anticancer applications. Thesis, Monash University Malaysia, Malaysia, 2015.
[6] Cui W., Chang J., Dalton P.D.: Electrospun Fibers for Drug Delivery. Compr Biomater 4 (2011) 445-462.
[7] Yi N.H.: Electrospun membranes of polylactic acid (PLA)/ polycaprolactone(PCL) encapsulated with drug loaded halloysite for sustained antimicrobial protection. Thesis, Monash University Malaysia, Malaysia, 2015.
[8] Nakielski P.: Systemy uwalniania leków oparte na nanowłóknach. PhD thesis, Instytut Podstawowych Problemów Techniki Polska Akademia Nauk, Warszawa, 2015.
[9] Kołbuk D.: Wpływ warunków elektroprzędzenia na strukturę i właściwości jedno- i dwuskładnikowych nanowłókien polimerowych stosowanych w inżynierii tkankowej. PhD thesis, Instytut Podstawowych Problemów Techniki Polska Akademia Nauk, Warszawa, 2012.
[10] Zhang C., Feng F., Zhang H.: Emulsion electrospinning: Fundamentals, food applications and prospects. Trends Food Sci. Technol. 80 (2018) 175-186.
[11] Miguel S.P. et al.: Electrospun polymeric nanofibres as wound dressings: A review. Colloids Surf. B Biointerfaces 169 (2018) 60-71.
[12] Yoo H.S., Kim T.G., Park T.G.: Surface-functionalized electrospun nanofibers for tissue engineering and drug delivery. Adv. Drug Deliv. Rev. 61, 12 (2009) 1033-1042.
[13] Sebe I., Szabó P., Kállai-Szabó P., Zelkó R.: Incorporating small molecules or biologics into nanofibers for optimized drug release: A review. Int. J. Pharm. 494, 1 (2015) 516-530.
[14] Cheng H., Yang X., Che X., Yang M., Zhai G.: Biomedical application and controlled drug release of electrospun fibrous materials. Mater. Sci. Eng. C, 90 (2018) 750-763.
[15] Radisavljevic A. et al.: Cefazolin-loaded polycaprolactone fibers produced via different electrospinning methods: Characterization, drug release and antibacterial effect. Eur. J. Pharm. Sci. 124 (2018) 26-36.
[16] Sultanova Z., Kaleli G., Kabay G., Mutlu M.: Controlled release of a hydrophilic drug from coaxially electrospun polycaprolactone nanofibers. Int. J. Pharm. 505, 1 (2016) 133-138.
[17] Alavarse A.C. et al.:Tetracycline hydrochloride-loaded electrospun nanofibers mats based on PVA and chitosan for wound dressing. Mater. Sci. Eng. C, 77 (2017) 271-281.
[18] Cejkova J., Cejka C., Trosan P., Zajicova A., Sykova E., Holan V.: Treatment of alkali-injured cornea by cyclosporine A-loaded electrospun nanofibers – An alternative mode of therapy. Exp. Eye Res. 147 (2016) 128-137.
[19] Coimbra P., Freitas J.P., Gonçalves T., Gil M.H., Figueiredo M.: Preparation of gentamicin sulfate eluting fiber mats by emulsion and by suspension electrospinning. Mater. Sci. Eng. C 94 (2019) 86-93.
[20] Moydeen A.M., Padusha M.S.A., Aboelfetoh E.F., Al-Deyab S.S., El-Newehy M.H.: Fabrication of electrospun poly(vinyl alcohol)/dextran nanofibers via emulsion process as drug delivery system: Kinetics and in vitro release study. Int. J. Biol. Macromol 116 (2018) 1250-1259.
[21] Katsogiannis K. A. G., Vladisavljević G. T., Georgiadou S.: Porous electrospun polycaprolactone (PCL) fibres by phase separation. Eur. Polym. J. 69 (2015) 284-295.
[22] Huang C., Thomas N. L.: Fabricating porous poly(lactic acid) fibres via electrospinning. Eur. Polym. J. 99 (2018) 464-476.

THE EFFECT OF TITANIUM DIOXIDE MODIFICATION ON THE COPPER POWDER BACTERICIDAL PROPERTIES

Małgorzata Rutkowska-Gorczyca[1]*, Justyna Molska[2], Dominika Grygier[1]

[1] Wroclaw University of Science and Technology, Department of Materials Science, Strength and Welding Technology, ul. Łukasiewicza 7-9, 50-371 Wrocław, Poland
[2] Wroclaw University of Science and Technology, Department of Vehicle Engineering, ul. Braci Gierymskich 164, 51-640 Wrocław, Poland
*e-mail: malgorzata.rutkowska-gorczyca@pwr.wroc.pl

Abstract

The bactericidal and bacteriostatic effects of copper have been known for a long time. However, the coatings apart from biological activity should fulfil a number of other requirements, such as tightness, scratch resistance or aesthetic appearance. Researchers have been working on creating durable coatings meeting these requirements for a long time. Scientific research indicates a high interest in active coatings. Nano-scale additives are used, with the aim to modify the material's performance at the atomic level. Composite coatings allow us to provide the materials multifunctionality, and in addition, can enhance their mutual action. There are many methods for creating such materials. One of the techniques of applying composite coatings is the Cold Spray method, in which the coating is made of a powder. The main purpose of the modification is to obtain a bactericidal and bacteriostatic effect, but also a durable and wear-resistant coating. The paper proposes modifications of copper powder with amorphous submicron titanium dioxide in order to increase its biological activity. The modified powder can be used to create coatings by various methods including thermal methods. The work presents a material analysis of Cu and TiO_2 powders and results of bactericidal tests carried out on a Cu-TiO_2 composite powder. The experiment included Escherichia coli and Staphylococcus aureus. The studies have shown a positive effect of the addition of TiO_2 on bactericidal properties against both Staphylococcus aureus (Gram-positive bacteria) and Escherichia coli (Gram-negative bacteria) when mixed with copper at 1:9 ratio.

Keywords: *composite powder, Cu, TiO_2, bactericidal tests*

[Engineering of Biomaterials 149 (2019) 15-19]

Introduction

Copper is known as an important micronutrient required in very small amounts for the survival of most aerobic organisms but at high concentrations can become toxic and inhibit microbial growth. Bogdanovic et al. [1] show that copper nanoparticles (Cu NPs) (diameter 5.3 nm) were able to reduce more than 98% of all tested strain (include *E. coli* and *S. aureus*) after 2 h of contact and Cu NPs has higher reduction rate for *E. coli* than *S. aureus*. Argueta-Figueroa et al. [2] also confirmed that Cu NPs have the antibacterial activity against *E. coli* and *S. aureus* (minimal inhibitory concentration, MIC = 1000 μg/ml) and cause more membrane damages of the *E. coli* as compared to *S. aureus*. The results of the experiment with another Gram-negative bacteria (*Salmonella*) showed that under dry incubation conditions bacterial cells are extremely vulnerable to copper [3]. He X. et al. [4] also shows that CuO/TiO_2 coating has high antibacterial activity against *S. aureus* in contrast to pure titanium and TiO_2 coating. It can be explained that the addition of copper is the crucial factor to endow copper/TiO_2 coating with the antibacterial effect against *S. aureus*. TiO_2 coating with the addition of copper enhanced antibacterial activity against *E. coli* and *S. aureus* [5].

The bactericidal and bacteriostatic effects of copper have been known for a long time, since then, researchers have been working on coatings that have these properties. The coatings apart from biological activity should fulfil a number of other requirements, such as tightness, scratch resistance or aesthetic appearance. The production of active composite materials with bactericidal activity is a very hot topic nowadays. The problem is, that currently known and applied Cu-TiO_2 protective layers are thick, heterogeneous and unstable. The composites based on copper and titanium dioxide have been tested several times, in most cases coatings in the form of nanopowders or thin films have been made. Sol-gel deposited Cu-TiO_2 films are not mechanically stable, in many cases their preparation is not reproducible, do not present uniformity but only low adhesion. Films obtained by a direct current magnetron sputtering, as reported, avoid the disadvantages of Cu-films prepared by sol-gel methods [6-8]. Ultra-thin copper/titanate coatings can be produced, among others, by the Highly Ionized Pulsed Plasma Magnetron Sputtering method (HIPMS), in which the bactericidal effect is activated by visible light. The study shows the first complete report on ultrathin TiO_2/Cu nano-particulate films leading to fast bacterial loss of viability. The TiO_2/Cu sputtered films induced complete bacteria *E. coli* inactivation in the dark, which was not observed in the case of TiO_2. When Cu was present, the bacterial inactivation was accelerated under low-intensity solar light and this may have a positive practical impact on biological technology. Disadvantages of HIPMS lead scientists to look for new technologies to complement these shortcomings. Cold spray technology, due to the low temperature during spraying, does not cause physicochemical changes in the modified material, also the plastic strain energy accompanying the formation of the coating does not cause phase changes in the coating [9].

In this study, we propose modifications of copper powder with amorphous submicron titanium dioxide in order to increase its biological activity. The modified powder can be used to create coatings by various methods including thermal methods. The work presents an analysis of Cu and TiO_2 powders and results of bactericidal tests carried out on a Cu-TiO_2 composite powder.

Materials and Methods

A dendritic commercial copper powder with a particle size of 10-100 μm obtained by the electrolytic method was used for the tests. The use of the dendritic form of the powder assures its better binding to the surface. However, such high surface area has a direct effect on the accelerated oxidation of the powder surface. The powder is characterized by different structure and size of dendritic particles as shown by scanning electron microscopy (SEM) observations (FIG. 1 a-d).

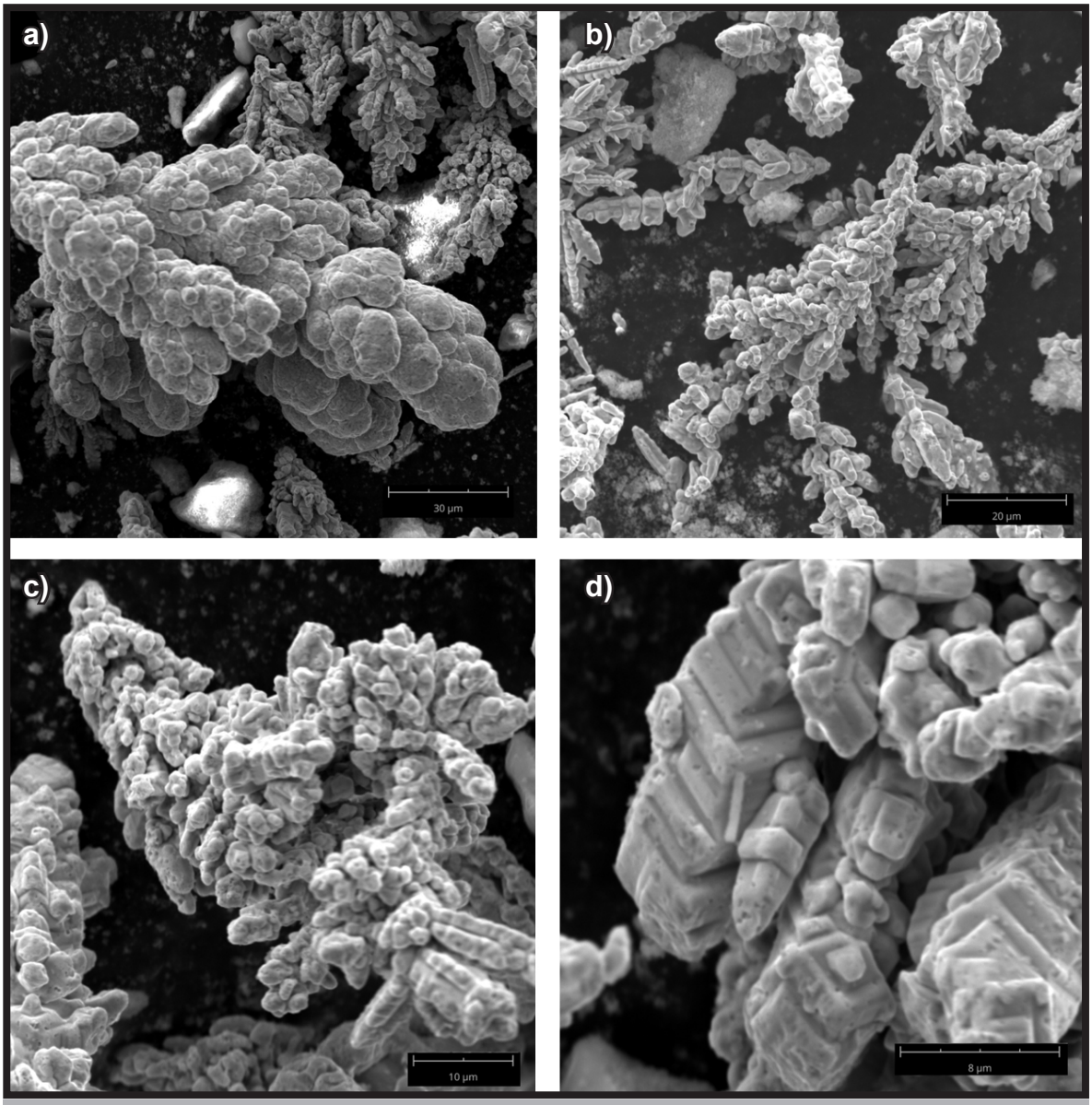

FIG. 1. a-d Different types of morphology of copper powder produced by electrolytic method studied by SEM.

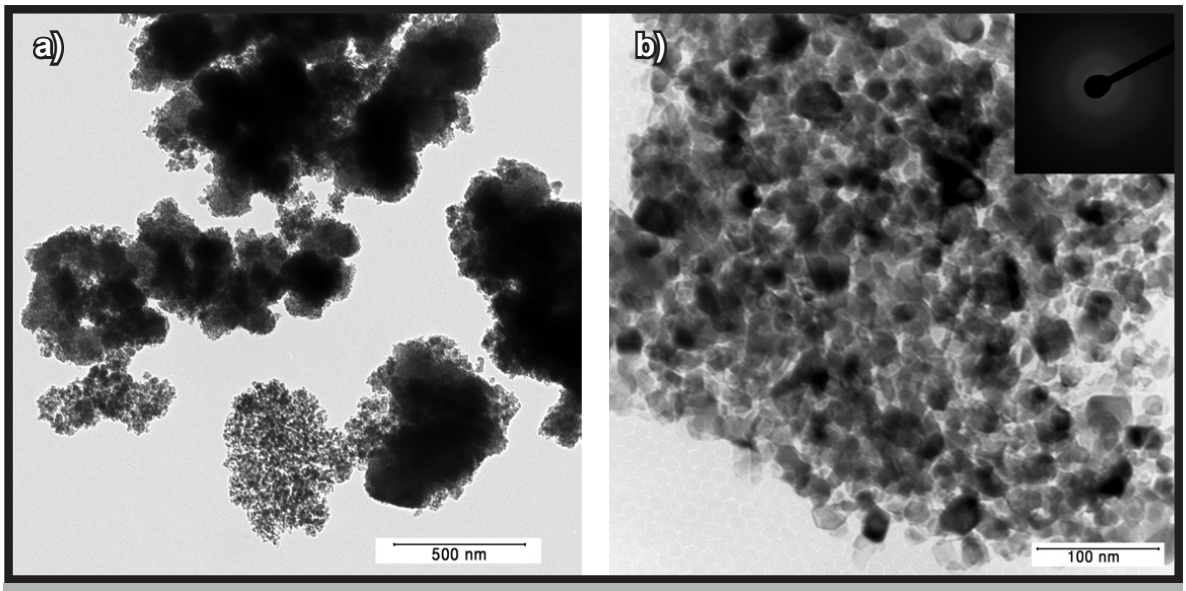

FIG. 2. a-b Morphology of titanium dioxide powder studied by TEM.

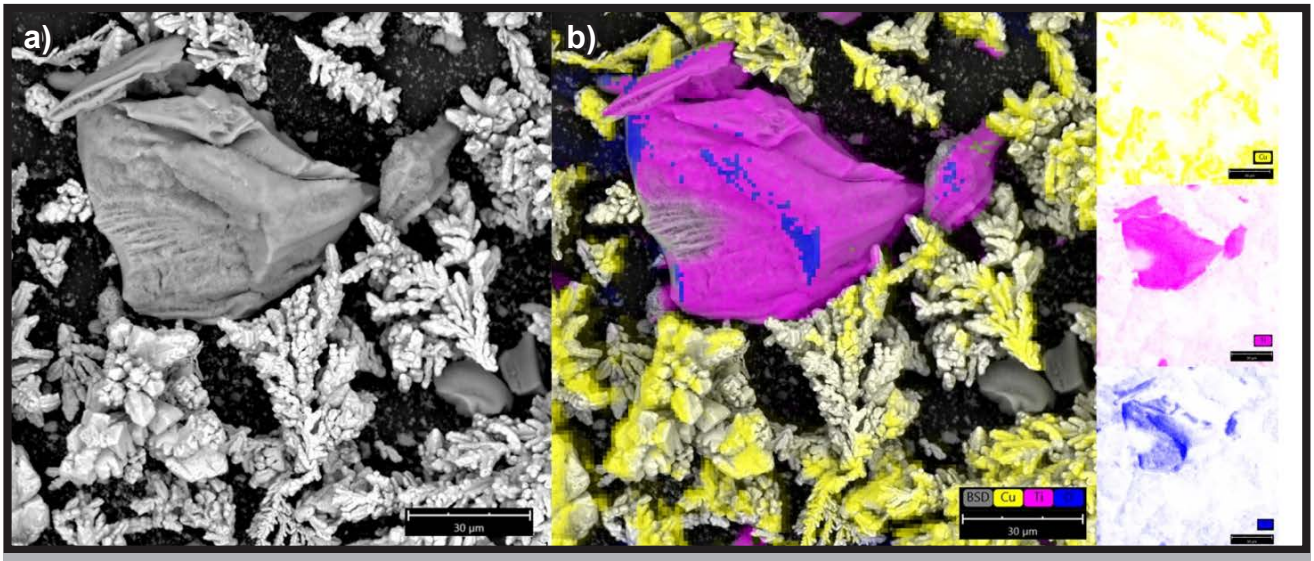

FIG. 3. SEM picture (a) and EDS elemental distribution (b) in composite powder with Cu-25TiO_2 composition.

The variety of structures has a positive effect on the formation of the coating during application using the Cold Spray method and coating deposition is much more efficient than the use of symmetrical spherical copper particles.

The powder of copper was mixed with submicron titanium dioxide powder produced by the sol-gel method at the Department of Mechanics and Materials Engineering at the Wroclaw University of Science and Technology [10]. TiO_2 powder of the amorphous type, which also possesses antibacterial activity properties, was used for the tests. The morphology of the TiO_2 powder has a diverse structure, both nanometric particle size and agglomerates with sizes of several dozen nanometres are visible in the transmission electron microscopy (TEM) pictures (FIG. 2 a,b). Diffraction analysis of TiO_2 powder confirmed the amorphous structure of the material (FIG. 2 b).

Four different concentrations of Cu and TiO_2 powders were used. The powders (Cu and TiO_2) were mixed in a mechanical stirrer for 4 h. Pure copper was used as a reference material, and further powders were additionally supplemented with 10, 25 and 50% mass concentrations of titanium dioxide. Analysis of the composition of the elements included in the powder showed that the titanium dioxide powder, despite the nanometric granulation, does not occupy the position between the branches of dendritic copper particles. The components of the composite powder form separate fractions despite intense mixing, which is visible on the map analysis of elements made by the electron dispersion spectroscopy (EDS) method (FIG. 3).

Zone inhibition assay is a qualitative method commonly used to measure antibiotic resistance, but also to test antimicrobial surfaces/substance properties. With this method, a pure bacterial culture is suspended in a buffer, standardized to a density (OD_{600}) and then spread over an agar plate. A filter-paper disk, impregnated with the compound (e.g. antibiotic), is placed on the surface of the agar. After required incubation time, which depends on a bacterial strain, the diameter of the zone of inhibition should be measured, including the diameter of the disc. If the bacterial strain is susceptible to the antimicrobial agent, then a zone of inhibition appears on the agar plate, if it is resistant to the antimicrobial agent, then no zone is observed.

Another method to determine the antibacterial effect is connected with MIC – minimal inhibition concentration. It can be done for aqueous samples using microplates or broth – 2-fold dilution are prepared for each concentration of the solution and then no microbial growth is observed. The lower concentration where no microbial growth is observed, the higher antimicrobial effect is. For plastic and non-porous surfaces, it can be also evaluated according to ISO Standard. Results are given as a difference in recovery of the bacterial inoculum after the incubation on the tested surface (shown in log10 or percentages).

The experiment included *E. coli* ATCC 11775 (Gram-negative bacteria) and *S. aureus* ATCC 6538P (Gram-positive bacteria), which were obtained from Polish Collection of Microorganisms (WFCC, No. 106). Strains were used after 24 h incubation at 37°C to prepare the inoculum to a concentration of 10^9 cfu/ml. A suspension of *S. aureus* and *E. coli* was sprayed over the total area of each Petri dish in triplicate. Then paper discs (7 mm diameter) soaked in a solution of a mixture of Cu-TiO_2 powders (10 mg/ml) were put on nutrient agar plates. After incubation at 35°C for 48 h, the diameter of the inhibition zone was measured by the calliper. The result equal to 7 mm is actually no zone of inhibition (no antimicrobial effect) as in the negative control.

The same bacterial inoculum was used to determine MIC (of an aqueous suspension of a mixture of Cu-TiO_2 powders (using broth suitable for bacteria growth). All solutions were prepared using sterile 96-well plate. 100 µl of nanoparticles suspension was added to each well according to the scheme shown in FIG. 4. The initial concentration of nanoparticles was 10 mg/ml and 2-fold dilutions were prepared from well number 1 to well number 7 (from 10 mg/ml to 156.25 µg/ml). Three types of control samples were prepared – broth without bacteria and nanoparticles (K-), broth with bacteria (K+) and nanoparticles suspended in broth (K_{Np}). The bacterial suspension (concentration – 10^9 cfu/ml) was added to each well (except control K-) and then incubated at 37°C for 24 h (with shaking). The optical density was measured using a Gen5 microplate reader at 600 nm. The results were given in MIC (mg/ml).

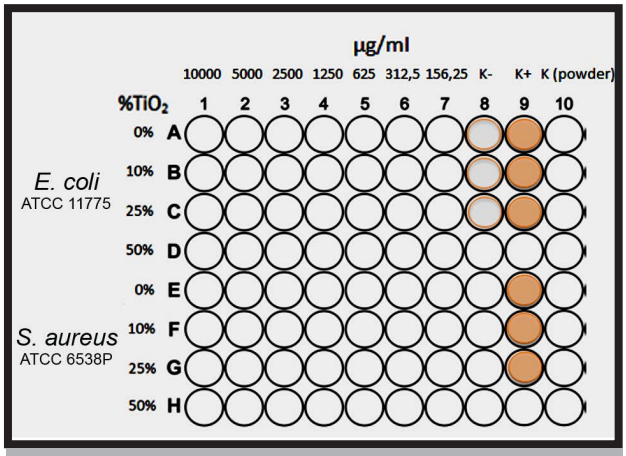

FIG. 4. Scheme of minimal inhibitory concentration test (MIC).

Results and Discussions

The analysis of the obtained results shows the beneficial effect of the addition of the titanium dioxide fraction on the microbiological activity of the copper powder against *S. aureus and E. coli*. The results of zone inhibition method are shown in TABLE 1 and TABLE 2.

Copper NPs and titanium dioxide at concentrations of titanium dioxide 10% and 25% show good inhibition zone against *E. coli and S. aureus.* There was no inhibition zone for titanium dioxide at a concentration 50% (FIG. 5). The best results were obtained for addition titanium dioxide at concentration 10% and 50% for both reference strains. The tests confirm the results obtained for TiO_2-Cu coatings produced by magnetron sputtering method where the authors found that addition of copper into titanium dioxide structure during sputtering process resulted in increasing antimicrobial activity for microorganisms (*E. coli, Bacillus subtilis, S. aureus, Enterococcus hirae* and *Candida albicans*) [11]. A significant effect on the test results and bactericidal activity could have been the oxidation state of the copper powder. The critical concentration of the modifying fraction seems to be very important in this method, it has a decisive influence on bactericidal properties.

In the microplate assay for determining MIC, there was no turbidity of broth in K- and K_{Np} control samples and noticeable turbidity in K+ control samples for *E. coli* and *S. aureus* strains, which confirm that the test was carried out properly. The results showed that a mixture of Cu-TiO_2 powders has higher antimicrobial efficacy against *S. aureus*. The MIC of mixtures of Cu-TiO_2 is varied, but the lowest was observed for Cu+10%TiO_2 samples for both reference bacteria strains (TABLE 3).

The lower concentration where no microbial growth is observed, the higher antimicrobial effect is. This test should be compared to the MBC (minimum bactericidal concentration), which is complementary to the MIC and also to the test according to ISO standard for antimicrobial efficiency of the surface.

TABLE 1. Zone of inhibition of Cu and TiO_2 powder against *E. coli* ATCC 11775.

	Diameter of inhibition zone [mm]		SD [mm]
Cu	*E. coli* ATCC 11775	10.47	0.32
Cu+10%TiO_2		10.27	0.99
Cu+25%TiO_2		11.87	1.86
Cu+50%TiO_2		0	-

TABLE 2. Zone of inhibition of Cu and TiO_2 powder against *S. aureus* ATCC 6538P.

	Diameter of inhibition zone [mm]		SD [mm]
Cu	*S. aureus* ATCC 6538P	10.34	0.37
Cu+10%TiO_2		11.37	0.85
Cu+25%TiO_2		12.28	0.56
Cu+50%TiO_2		0	-

TABLE 3. MIC (minimal inhibitory concentration) of Cu and TiO_2 powder (*E. coli* ATCC 11775, *S. aureus* ATCC 6538P).

	MIC, mg/ml	
Cu	*E. coli* ATCC 11775	2.5
Cu+10%TiO_2		0.625
Cu+25%TiO_2		10
Cu+50%TiO_2		>10
Cu	*S. aureus* ATCC 6538P	2.5
Cu+10%TiO_2		0.625
Cu+25%TiO_2		5
Cu+50%TiO_2		>10

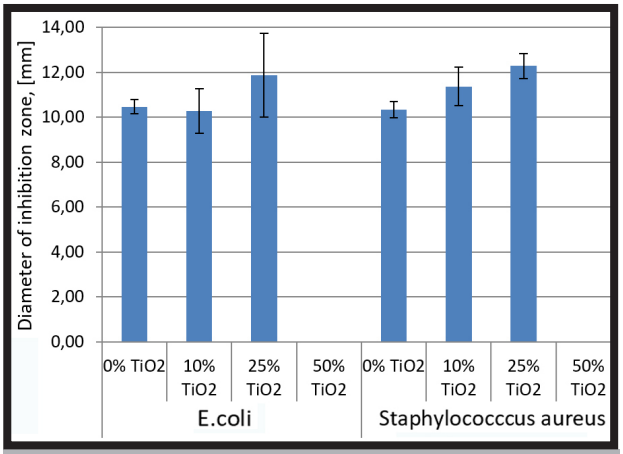

FIG. 5. Influence of the addition of titanium dioxide on bactericidal activity of copper powder.

Conclusions

The tests were carried out on copper powders modified with the amorphous fraction of titanium dioxide at various concentrations: 10, 25 and 50%. The bacterial strain *E. coli* ATCC 11775 and *S. aureus* ATCC 6538P were used for microbiological tests. The research involved the determination of the impact of the modification on the inhibition zone of bacterial proliferation after 48 h of exposure and also determination of MIC (minimal inhibitory concentration) of an aqueous suspension of a mixture of Cu-TiO_2 powders in conditions of 37°C for 24 h (with shaking). The studies showed a positive effect of the modification primarily against reference bacteria strains (*E. coli* and *S. aureus*). In both tests, the results clearly indicate that the addition of titanium dioxide at a concentration of 10% and 25% is beneficial. It seems reasonable to develop an optimal concentration of modifying TiO_2 fraction for individual bacterial strains, in order to obtain sufficiently high-performance antibacterial properties.

Acknowledgements

This work was financed by the statutory research of Faculty of Mechanical Engineering, Wroclaw University of Science and Technology, Poland.

References

[1] Bogdanović U., Lazić V., Vodnik V., Budimir M., Markovic Z., Dimitrijewic S.: Copper nanoparticles with high antimicrobial activity. Materials Letters 128 (2014) 75–78.
[2] Argueta-Figueroa L., Morales-Luckie A., Scougall-Vilchis J., Olea-Mejia O.F.: Synthesis, characterization and antibacterial activity of copper, nickel and bimetallic Cu–Ni nanoparticles for potential use in dental materials. Progress in Natural Science: Materials International 24 (2014) 321–328.
[3] Zhu L., Elguindi J., Rensing C., Ravishankar S.: Antimicrobial activity of different copper alloy surfaces against copper resistant and sensitive Salmonella enterica. Food Microbiology (2013) 303-10.
[4] He X., Zhang G., Wang X., Ruiqiang Hang R., Huang X., Qin L., Tang B., Zhang X.: Biocompatibility, corrosion resistance and antibacterial activity of TiO_2/CuO coating on titanium. Ceramics International 43 (2017) 16185–16195.
[5] Chen S., Guo Y., Zhong H., Chen S., Li J., Ge Z.: Synergistic antibacterial mechanism and coating application of copper/titanium dioxide nanoparticles. Chemical Engineering Journal 256 (2014) 238-246.
[6] Maness P.C., Smolinski S., Blake D.M., Huang Z., Wolfrum E.J., Jacoby W.A.: Bactericidal activity of photocatalytic TiO_2 reaction: toward an understanding of its killing mechanism. Applied and Environmental Microbiology 65 (1999) 4094–4098.
[7] Rtimi S., Oualid B., Pulgarin C., Lavanchy J., Kiwi J.: Growth of TiO_2/Cu films by HiPIMS for accelerated bacterial loss of viability. Surface & Coatings Technology 232 (2013) 804-813.
[8] Rtimi S., Pulgarin C., Baghriche O., Kiwi J.: Accelerated bacterial inactivation obtained by HIPIMS sputtering on low cost surfaces with concomitant reduction in the metal / semiconductor content. RSC Advances 3(32) (2013) 13127-13130.
[9] Winnicki M., Małachowska A., Baszczuk A., Rutkowska-Gorczyca M., Kukla D., Lachowicz M., Ambroziak A.: Corrosion protection and electrical conductivity of copper coatings deposited by low-pressure cold spraying. Surface & Coatings Technology 318 (2017) 90-98.
[10] Baszczuk A., Jasiorski M., Borak B., Wódka J.: Insights into the multistep transformation of titanate nanotubes into nanowires and nanoribbons. Materials Science-Poland 34(4) (2016) 691-702.
[11] Wojcieszak D., Mazur M., Kaczmarek D., Poniedziałek A., Osękowska M.: An impact of the copper additive on photocatalytic and bactericidal properties of TiO_2 thin films. Materials Science 35 (2017) 421-426.

PRELIMINARY INVESTIGATIONS ON SILICONE RESIN COMPOSITES WITH CARBON FILLER FOR DRY ELECTRODES APPLICATION

Dominik Grochala[1]*, Marcin Kajor[1], Paweł Smoleń[2], Ewa Stodolak-Zych[3]

[1] AGH University of Science and Technology, Faculty of Electrical Engineering, Automatics, Computer Science and Biomedical Engineering, al. A. Mickiewicza 30, 30-059 Kraków, Poland
[2] Smart Nanotechnologies S.A., K. Olszewskiego St. 25, 32-566 Alwernia, Poland
[3] AGH University of Science and Technology, Faculty of Materials Science and Ceramics, al. A. Mickiewicza 30, 30-059 Kraków, Poland
*e-mail: grochala@agh.edu.pl

Abstract

The paper presents results of investigations of basic material properties of novel composites based on silicone resin and carbon nanotubes as a filler. The motivation for the research is a need for materials which provide better mechanical properties than standard wet Ag/AgCl electrodes. However, a critical issue is also obtaining defined electrical characteristics in order to preserve an ability to effectively record biomedical signals such as electrocardiography (ECG). Within the introduction chapter, related researches and the current state-of-the-art in the context of dry electrodes technology were described. In the next step technological aspects of components processing and forming as well as the morphology of substrates used in the research were presented. Thermally-cured silicone resin was utilized to obtain elastic properties of the resulting material. The carbon nanotubes (CNT) were chosen as a conductive medium which provides defined electrical impedance. A developed technological process allowed to deliver samples of reproducible structure and properties. In the next chapter, methods and results of conducted experiments involving electrical, mechanical and thermal examination were presented. Finally, achieved outcomes are promising in the context of improvements of the designed composite. Especially the conductivity below 100 Ohms constitutes a significant motivation for further research in the field of dry electrodes for biosignals acquisition.

Keywords: *dry electrodes, ECG pads, silicone resin, carbon filler*

[Engineering of Biomaterials 149 (2019) 20-24]

Introduction

Nowadays, aging society struggling with rapid and stressful lifestyle suffers from civilization diseases paradoxically, especially in well-developed western countries. On the other hand, heart diseases constitute a major part of deaths worldwide. It has been calculated that almost two thousand people die each day because of cardiac disorders [1]. This gives the motivation to utilize top-notch technologies to provide sophisticated yet convenient medical services supporting the elderly and chronically ill patients. One example of emerging technology which seems to meet requirements of modern healthcare needs is telemedicine which combines achievements of multiple scientific branches such as electronics, computer science, and material engineering. This approach aims to provide remote medical services even in domestic conditions by utilizing wearable sensors which send physiological signals directly from households to medical facilities. Physicians may then analyze provided diagnostic data and decide if there is a need for any medical intervention. One of the major challenges is, however, a design of electrodes capable of capturing biosignals generated on the body surface as a result of heart activity or muscle movement. The issue of biopotential monitoring is definitely a complex challenge mainly due to the skin-electrode interface. From the theoretical point of view, the phenomenon which contributes significantly to the electrical properties of a conductor is a Helmholtz double layer. This effect is caused by ion separation and occurs on the contact between electrolyte and conductive medium. In practical application, it results in capacitance in the electrical circuit [2]. This problem can be effectively compensated by the use of wet chloride silver electrodes, however, some applications, e.g. textile-integrated solutions are still an area of development and improvements in the context of advanced materials. Apart from adjusting the interface resistance, the next vital aspect of electrode design is undoubtedly a need to ensure biocompatibility and application properties like formability or adhesion to other media. This gives a motivation to utilize recent advances in material science to find a solution which would be more efficient than traditional Ag-AgCl electrolyte electrodes for electrocardiography (ECG) measurement. It turns out that when used over an extended time period, wet electrodes tend to cause skin irritation and change electrical properties which may lead to reducing of a signal-to-noise ratio. Such side effects may be limited by dry composite electrodes. This was proved by investigating the performance of self-adhesive carbon nanotubes/adhesive polydimethylsiloxane (CNT/aPDMS) electrodes in a real long-term ECG measurement by Jaehyo Jung et al. [3]. Julia W.Y. Kam et al. also delivered a comparison of standard gel pads and novel metallic dry electrodes. Apart from superior mechanical properties and increased patient's comfort the latter also allowed to obtain reliable ECG signal. This was proved by significant positive correlation ratios (r = 0.54-0.89) of electrophysiological metrics calculated for these two independent systems [4]. Carbon nanotubes are willingly used as a nanofiller in various polymer compositions in particular - in conductive plastics applications. This approach is suitable in biomedical electrodes design. Adaptation of material properties can be achieved by surface modification of a filler [5]. Il-Seok Park et al. examined the impact of multiwall carbon nanotubes (MWCNT) addition on magnetic and mechanical properties of silicone elastomer-based composite. In this research, the carbon filler with an average thickness of 10 nm and over 95% purity was used. Authors applied only three concentrations of CNTs (0.2 wt%, 0.5 wt%, 0.7 wt%) as larger amounts of MWCNT caused difficulties in homogenization.

This research proved that proposed composites manifest interesting changes in mechanical and dielectric properties (particularly for the highest CNTs concentration) which makes them useful as dampers and actuator elements [6]. It was also confirmed that the use of MWCNT as an additive gives better results in comparison with carbon black (CB). M. Norkhairunnisa et al. tested 0.5 to 2% vol. concentration of carbon fillers in PDMS elastomer. One of the biggest difficulties in material preparation was an uneven distribution of CNT due to the formation of agglomerates. In this case conductivity plateau of -2.62 log σ[S/cm] was reached at 2% concentration of MWCNT. To achieve a similar result for CB a volume of 2.5% was needed. Another useful property of the CNT based composite is an increased thermal conductivity. However, as the authors concluded, preparation and surface treatment of MWCNT is very important to improve the properties of a final composite [7]. Jeong Hun Kim et al. proposed a universal flexible and conductive material for wearable applications. They developed new polydimethylsiloxane (PDMS) based composite with a CNT filler. Homogenic character of CNT dispersion in the matrix is crucial for electrical properties of final samples. They used isopropylic alcohol as a carbon filler solvent which was next evaporated from the mixture. This type of composite can be used in different applications including a flexible conductor which can replace wires in wearable electronics. Furthermore, a variable and strain-dependent resistance makes this material useful for mechanical sensors elements design. Research also proved that biopotential electrodes made of proposed composite have properties desired in such applications. To investigate this further, ECG signals were recorded for 7 days with PDMS+CNTs conductive pads. No deterioration in terms of a signal quality was found in comparison with standard Ag/C electrodes [8].

This study aims to provide a preliminary investigation of a new kind of composite dry electrodes. The best effect for the chosen application is provided by carbon nanotubes because in addition to excellent electrical properties CNTs provide better mechanical properties, which is not obtained in the case of amorphous carbon with a spherical structure. To verify the usability and durability of the proposed solution we conducted a set of material tests including electrical impedance and mechanical tensile strength measurements as well as verification of antibacterial properties.

Materials and Methods

As the carbon additive that was aimed to provide a conductivity of polymer matrix the commercially available multiwall carbon nanotubes (MWCNTs) (CNT Co., Ltd., Korea) were used. This powder component is obtained by catalytic chemical vapour deposition method using Fe catalyst. Carbon purity in raw multiwall carbon nanotubes was at least 95%. Before using, carbon nanotubes were chemically purified by heating under reflux in a mixture of boiling, concentrated sulfuric acids (VI) (98%) (Stanlab, Poland) and nitric acid (V) (65%) (Stanlab, Poland) in a ratio of 1:3 for about 16 h to completely remove amorphous carbon and traces of catalysts and to oxidize nanotubes' surface and obtain polar functional groups with a predominance of carboxyl groups. In turn, carboxylic groups were attached to the ends and walls of CNTs. The oxidized carbon nanotubes were eluted with demineralized water and ethanol until filtrate pH was stabilized. Used nanotubes had a diameter ranging from 10-40 nm and length in the range of 1-25 μm. For MWCNTs observation and their morphology the Field Emission Scanning Electron Microscope JEOL JSM- 7800F was used. The instrument has a field emission gun and is also equipped with an EDX (energy dispersive X-ray) detector for chemical analysis and a STEM (Scanning Transmission Electron Microscopy). The analysis was carried out with an accelerating voltage of 30 kV. Results in the form of pictures were taken in a bright field. Nanopowder of MWCNTs, used as a carbon nanofiller, was added to ethanol and exposed to ultrasonic waves. For TEM method, one drop of the suspension was placed on a copper 300 mesh grid coated with holey carbon film. Then the sample was dehydrated at 40°C.

The polymer matrix was obtained by mixing hydroxy functional polydimethyl siloxane polymer (Elastomer 80N, Wacker, Germany) and high-temperature vulcanizing silicon rubber (Polsil Gum 100/30, Silikony Polskie, Poland). Both components were mixed together at a ratio of 5:4. The preliminary part of this research included also the design of the technological process of obtaining samples of defined geometry in laboratory conditions. The viscosity of used polymeric components implied a necessity to find a method to achieve a homogeneous structure of the final composition. After many trials, a laboratory triple roller was used to mix components together. This device contains three independent shafts moving axially in opposite phase driven by an electric motor. The gap between rollers can be easily adjusted to obtain optimal friction generated between moving parts and material being processed. Each polymer substrate was dispensed one after another onto the first shaft and proceeded through all moving parts until obtaining homogeneous and consistent composition (FIG. 1).

FIG. 1. Silicone matrix with carbon additive during preprocessing on a triple roller.

After thorough mixing, purified multi-wall carbon nanotubes in various concentrations were added into the polymer premix. After homogenization, a crosslinking system dedicated to polysiloxanes based on hydrogen siloxane-co-dimethylsiloxane was added to the mixing matrix. This substrate consisted of an inhibitor based on 3,5-dimethyl-3-hexanol and a platinum addition polymer catalyst (all Evonik, Germany). Finally, samples with three concentrations of the nanofiller were obtained: "1" – 10 wt%, "2" – 7.5 wt%, "3" – 5 wt%. The next step involved forming samples between Teflon plates in the hydraulic press under a load of approximately 1.5 tons at room temperature. In the following part rectangles of the size of 20 x 40 mm were cut from flat samples and immediately placed between Teflon separators in a steel die with an electric heater connected. One part of the samples was then formed and crosslinked in a hydraulic press under a load of 5 tons at 150°C for 30 min. The second part was placed in an incubator under a pressure generated by steel blocks at 150°C (45 min).

TABLE 1. Characteristics of materials resistance measured in DC.

Sample	R [Ω] 1. pad	R [Ω] 2. pad	R [Ω] 3. pad	R [Ω] mean	σ [S/m]
10% hot pressing	4.36	3.64	1.56	3.19	2.63
7.5% hot pressing	1.38	5.43	3.92	3.58	2.98
5% hot pressing	80.54	72.78	68.61	73.98	0.12
10% crosslinking in oven	14.80	1.34	2.91	6.35	0.74
7.5% crosslinking in oven	4.42	1.21	4.85	3.49	1.57
5% crosslinking in oven	83.26	61.65	72.43	72.45	0.05

In the next step, a basic electrical study was carried out to verify the usefulness of obtained samples as electrode materials. Keysight 34461A multimeter as 4-wire ohmmeter was used to directly measure direct current (DC) resistance (TABLE 1). The same device was applied as an ammeter in the alternating current (AC) setup. For impedance measurements, a functional generator SIGLENT SDG1025 was utilized as a sinusoidal signal source and Boonton 1130 analyzer for voltage measurement. Both devices were connected in a standard voltmeter-ammeter method configuration.

In this examination, three different carbon filler concentrations and two manufacturing methods (hot pressing and cold forming with crosslinking in an oven) were investigated. Then three pads from each forming/composition variant were cut out to increase accuracy and verify the bulk homogeneity. First, DC resistance was measured which was a base for calculation of conductivity of the material. AC parameters were also recorded. Two flat, square-shaped copper electrodes were prepared for measurements by soldering the connecting wires (FIG. 2). Samples were then placed between electrodes and the measurements were taken under a static load of 1 kg (perpendicular to the surface of the sample).

Mechanical testing of the composites was performed using Zwick-1435 machine with strips samples (5 x 80 mm). All materials were compared for tensile strength (Rm) and Young's modulus (E). The behavior of materials under *in vitro* conditions was checked, keeping them for 7 days in 0.9% NaCl and the effect of the environment on the mechanical properties of the materials was determined. The durability conditions for testing of the materials for dry electrodes were chosen for the duration of the device during the long-term ECG test.

The composite material was also microbiologically tested by contacting it with bacteria *E.coli* using Kriba-Miller test (agar/24 h). The aim of this experiment was to check possible antibacterial properties that may be an effect of the introduction of CNTs into the polymer matrix.

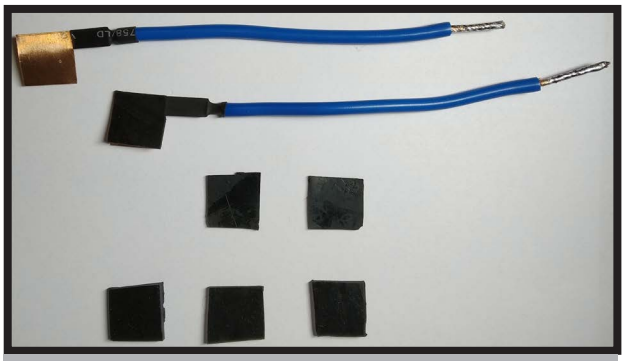

FIG. 2. Copper electrodes and cut pads of the composite samples.

Result and Discussion

The carbon nanofiller's morphology from the STEM is presented in FIG. 3. The analysis shows that the used nanotubes have a diameter smaller than 40 nm, which is consistent with the producer declaration. The declared length was not confirmed due to method limitations.

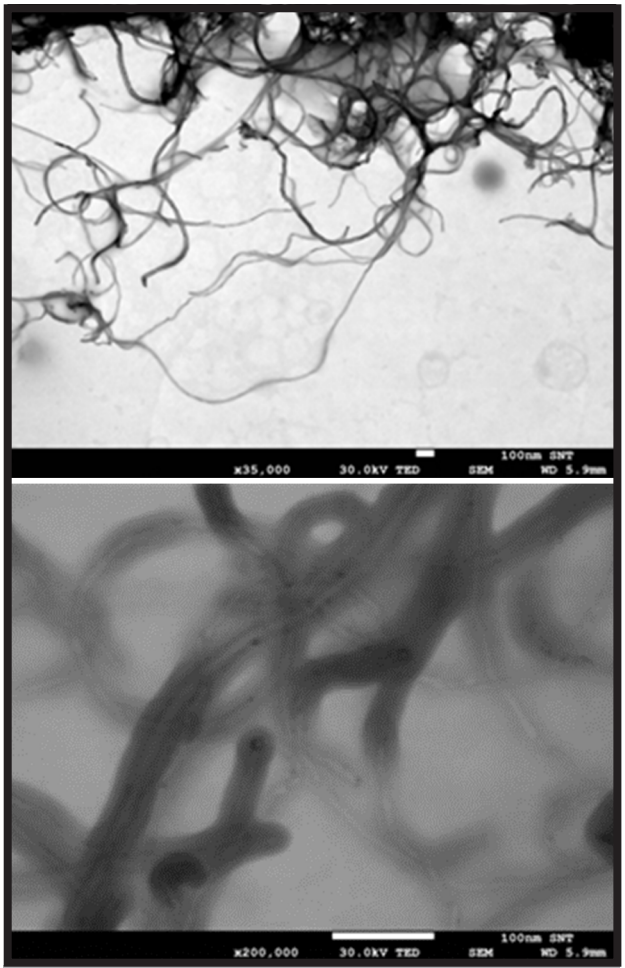

FIG. 3. STEM micrographs of multiwall carbon nanotubes (MWCNTs).

Mechanical properties

A set of the hot-pressed samples was tested for mechanical properties such as Young's modulus (E) and tensile strength (Rm). Low values of the standard deviation indicated homogeneous filler distribution in the resin. The filler concentrations (10 wt%, 7.5 wt%, 5 wt%) were selected based on the previous experiments with mixing process and optimized.

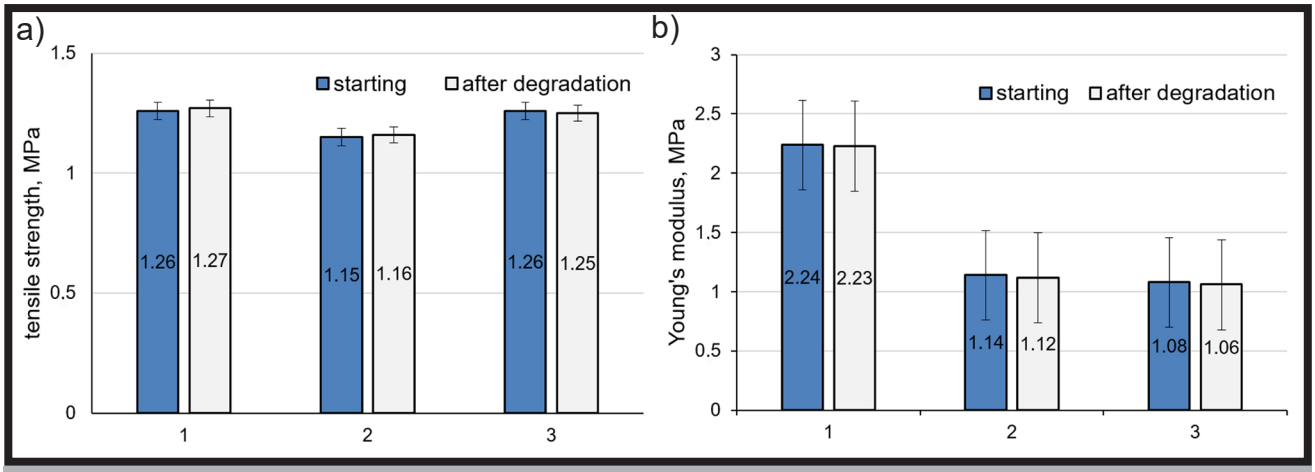

FIG. 4. Comparison of mechanical properties of the starting materials and materials after the degradation (7 days/37°C/0.9% NaCl): a) tensile strength, b) Young's modulus. ("1" – 10 wt% MWCNT, "2" – 7.5 wt% MWCNT, "3" – 5 wt% MWCNT)

TABLE 2. Characteristics of materials impedance measured in AC.

Sample	|Z| Ω 10Hz	|Z| Ω 100Hz	|Z| Ω 1000Hz	|Z| Ω 10000Hz
10% hot pressing	0.85	0.58	0.63	0.54
7.5% hot pressing	1.58	1.00	1.18	1.37
5% hot pressing	95.78	49.36	37.20	37.08
10% crosslinking in oven	3.28	2.71	3.23	3.47
7.5% crosslinking in oven	1.22	1.15	0.94	1.12
5% crosslinking in oven	26.07	24.44	29.33	46.21

Addition of 10 wt% of MWCNT resulted in a significant increase in Young's modulus and material stiffness, which can cause its breaking and crushing during exploitation. Both materials (5 wt% and 7.5 wt% MWCNT) had similar strength and significantly lower Young's modulus values. Despite the above observation, all tested materials had properties that allow their application as dry electrodes. Tensile strength was measured before and after the incubation in solution simulating degradation environment (contact skin – electrode, 0.9% NaCl) to determine durability of the proposed material. This *in vitro* experiment was carried out using a saline solution, which is similar to human sweat. Results show that no degradation was observed (FIG. 4). All materials which work as a dry electrode were stable under *in vitro* conditions.

Electrical parameters

Obtained results indicated a variation of parameters between samples that were formed in a cold press and crosslinked in a laboratory oven. The electrical conductivity of all samples was in a range from 0.05 to 2.98 S/m (TABLE 1) which is sufficient result for electrode applications [9]. The number of frequency data points in AC investigation might not be enough to fully represent the conductivity mechanism but this test was performed only to verify a bandwidth from the viewpoint of biosignals acquisition. The measured spectrum range was between 10 Hz and 10 kHz which corresponds to biopotential nature. Resulting linear characteristics indicate the lack of reactance part in the impedance (TABLE 2), which is desired in the context of reliable electrical biosignal acquisition.

Microbiological properties

Bacteria seeded on an agar medium and then cultured in vitro for 24 h/42°C were contacted with the tested materials. Due to the thickness of plastics (above 400 μm), the non-standard sizes of the samples submitted for testing were used. The test materials were kept in contact with the bacteria for 24 h and then the form of the bacterial biofilm was assessed (FIG. 5). In the literature, there are reports on the bactericidal properties of MWCNT [10-11]. Considering the long working time of the electrode applied directly to the human skin, the antibacterial properties of the electrodes would be desirable. Unfortunately, the results of the study indicated that the materials do not have antibacterial properties. After the set time of the experiment, a uniform bacterial layer appeared on all materials (FIG 5). In order to obtain antibacterial properties for the polymer matrix, it would be necessary to introduce proven additives with a bactericidal effect, e.g. nanometric silver [12].

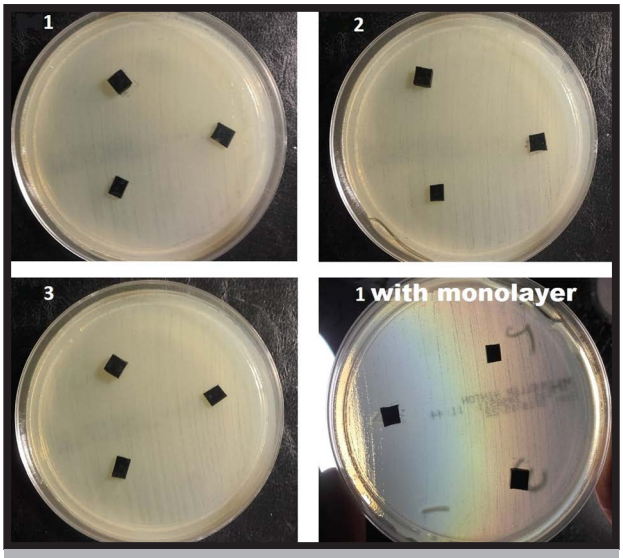

FIG. 5. Microbiological testing; no inhibition zone for bacteria *E.coli.*

Conclusions

Application of a carbon nanofiller such as graphite oxide, graphite, carbon nanotubes, graphene enabled to obtain a conductive polymer material with satisfactory mechanical properties. Results of breaking strength, deformation resistance and Young's modulus tests of the samples after degradation suggest that this material can be integrated with textiles.

A designed technology of processing of the proposed substrates allows to prepare in laboratory conditions a composite material with high CNTs homogenization in the silicone resin. A fact that the nanofiller was very evenly dispersed in the polymer matrix was proven by repetitive results of the mechanical tests. It turns out that, besides the addition of the carbon nanotubes also curing methodology has a significant impact on the resulting electrical properties. None of the prepared samples have antibacterial properties. However, the proposed material is certainly durable in the *in vivo* conditions. In the future, it is planned to conduct further research on the designed composite in the context of electrophysiological applications. Measured resistance of the tested samples was several ohms and featured linear bandwidth in a biopotential range. These results meet requirements for dry electrodes. On the other hand, the obtained material composition and its properties make it a promising alternative to the current standard solutions based on wet electrodes.

Acknowledgments

The work was carried out as part of the scientific cooperation between AGH University of Science and Technology, Faculty of Electrical Engineering, Automatics, Computer Science and Biomedical Engineering and Smart Nanotechnologies S.A.

References

[1] Azra'ai R.A., bin Taib M.N., Tahir N.M.: Artificial neural network for identification of heart problem. In Signal Processing and Communication Systems ICSPCS 2008. 2nd International Conference on Signal Processing and Communication Systems, 15-17 December 2008, Australia, Gold Coast, 1-6.

[2] Chi Y.M., Jung T.P., Cauwenberghs G.: Dry-contact and noncontact biopotential electrodes: Methodological review. IEEE reviews in biomedical engineering 3 (2010) 106-119.

[3] Jung J., Shin S., Kim Y.T.: Dry electrode made from carbon nanotubes for continuous recording of bio-signals. Microelectronic Engineering 203 (2019) 25-30.

[4] Kam J.W.Y., Griffin S., Shen A., Patel S., Hinrichs H., Heinze H.J., Deouell L.Y., Knight R.T.: Systematic comparison between a wireless EEG system with dry electrodes and a wired EEG system with wet electrodes. Neuroimage 1(184) (2019) 119-129.

[5] Karabiberoğlu Ş.U., Koçak Ç.C., Dursun Z.: Carbon Nanotube--Conducting Polymer Composites as Electrode Material in Electroanalytical Applications. In book: Carbon Nanotubes-Current Progress of their Polymer Composites. InTech (2016). DOI: 10.5772/62882

[6] Park I.S., Kim K.J., Nam J.D., Lee J., Yim W.: Mechanical, dielectric, and magnetic properties of the silicone elastomer with multi-walled carbon nanotubes as a nanofiller. Polymer Engineering & Science 47(9) (2007) 1396-1405.

[7] Norkhairunnisa M., Azizan A., Mariatti M., Ismail H., Sim L.C.: Thermal stability and electrical behavior of polydimethylsiloxane nanocomposites with carbon nanotubes and carbon black fillers. Journal of Composite Materials 46(8) (2012) 903-910.

[8] Kim J.H., Hwang J.Y., Hwang H.R., Kim H.S., Lee J.H., Seo J.W., Lee S.H.: Simple and cost-effective method of highly conductive and elastic carbon nanotube/polydimethylsiloxane composite for wearable electronics. Scientific reports 8(1) (2018) 1375.

[9] Marszałek Z., Gawędzki W.: Nowa metoda monitorowania stanu kontaktu elektrody biomedycznej ze skórą pacjenta. Przegląd Elektrotechniczny 90(5) (2014). 94-97.

[10] Siyu W., Yumei L., Rui Z., Toufeng J.: Chitosan surface modified electrospun poly(ε-caprolactone)/carbon nanotube composite fibers with enhanced mechanical, cell proliferation and antibacterial properties. International Journal of Biological Macromolecules 104, Part A (2017) 708-715.

[11] Usman Farid M., Khalid Khanzada N., Kyoungjin A.: An understanding fouling dynamics on functionalized CNT-based membranes: Mechanisms and reversibility, Desalination 456 (2019) 74-84.

[12] Javeria Kazmi S.M., Shehzad A., Mehmood S., Yasar M., Bhatti A.S.: Effect of varied Ag nanoparticles functionalized CNTs on its anti-bacterial activity against E. coli. Sensors and Actuators A: Physical 216(1) (2014) 287-294.